ABSTRACT

ARSHAD, AZKA. Photophysics of Metalloporphyrin Photosensitizers: Homomolecular Triplet-Triplet Annihilation. (Under the direction of Dr. Felix N. Castellano).

Metalloporphyrins are ubiquitous in their applications as triplet photosensitizers, particularly for promoting sensitized photochemical upconversion processes. In this thesis, bimolecular excited state triplet-triplet quenching kinetics, termed homomolecular triplet-triplet annihilation (HTTA), exhibited by the traditional triplet photosensitizers – zinc(II) tetraphenylporphyrin (ZnTPP), palladium(II) octaethylporphyrin (PdOEP), platinum(II) octaethylporphyrin (PtOEP), and platinum(II) tetraphenyltetrabenzoporphyrin (PtTPBP) – was revealed using conventional transient absorption spectroscopy. Nickel(II) tetraphenylporphyrin was used as a control sample as it is known to be rapidly quenched intramolecularly through ligand-field state deactivation and, therefore, cannot result in triplet-triplet annihilation (TTA).

The single wavelength transients associated with the metalloporphyrin triplet excited state decay – measured as a function of incident laser pulse energy in toluene – were well modeled using parallel first- and second-order kinetics, consistent with HTTA being operable. The combined transient kinetic data enabled the determination of the first-order rate constants (k_T) for excited triplet decay in ZnTPP (4.0×10^3 s^{-1}), PdOEP (3.6×10^3 s^{-1}), PtOEP (1.2×10^4 s^{-1}), and PtTPBP (2.1×10^4 s^{-1}) as well as the second-order rate constant (k_{TT}) for HTTA in ZnTPP (5.5×10^9 $M^{-1}s^{-1}$), PdOEP (1.1×10^{10} $M^{-1}s^{-1}$), PtOEP (7.1×10^9 $M^{-1}s^{-1}$), and PtTPBP (1.6×10^{10} $M^{-1}s^{-1}$).

In addition to the kinetic analysis, this thesis provides revised or previously unreported triplet excited state extinction coefficients for these metalloporphyrins, determined through ultrafast transient absorption spectroscopy and singlet depletion. These include ZnTPP (78,000 $M^{-1}cm^{-1}$ at

470 nm), PdOEP (67,000 $M^{-1}cm^{-1}$ at 430 nm), PtOEP (51,000 $M^{-1}cm^{-1}$ at 418 nm), and PtTPBP (100,000 $M^{-1}cm^{-1}$ at 460 nm).

The comprehensive experimental findings establish competitive timescales for homo- and heteromolecular TTA rate constants, implying the significance of considering HTTA processes in future research endeavors harnessing TTA photochemistry using common metalloporphyrin photosensitizers.

© Copyright 2025 by Azka Arshad

All Rights Reserved

Photophysics of Metalloporphyrin Photosensitizers: Homomolecular Triplet-Triplet Annihilation

by
Azka Arshad

A thesis submitted to the Graduate Faculty of
North Carolina State University
in partial fulfillment of the
requirements for the degree of
Master of Science

Chemistry

Raleigh, North Carolina
2025

APPROVED BY:

_____	_____
Dr. Felix N. Castellano Committee Chair	Dr. Elena Jakubikova
_____	
Dr. Reza Ghiladi	

DEDICATION

To my beloved maternal grandmother, *Masoom Begum*, whose wisdom and love are a source of guidance and strength for me for as long as I live.

BIOGRAPHY

Azka is the eldest of her three siblings and was born and raised in Lahore, the 2nd largest city in Pakistan and the 26th largest city in the world. She completed her BS in Chemistry at the Syed Babar Ali School of Science and Engineering at the Lahore University of Management Sciences (LUMS) in 2021. Her undergraduate research focused on the design and development of reduction-sensitive polymer-drug conjugates for targeted delivery of anticancer therapeutics under the supervision of Dr. Basit Yameen. In August 2021, Azka joined North Carolina State University as a Ph.D. student, where she now works under the supervision of Prof. Felix N. Castellano. In the Castellano lab, as part of the group's mission, Azka is committed to comprehending and potentially manipulating excited state dynamics to make significant strides in this field. Her research is focused on the photophysics and photochemistry of photosensitizers involved in homomolecular triplet-triplet annihilation and its application in photochemical transformations. This entails using spectroscopic methods to gain a detailed understanding of this process. Additionally, she aims to simplify further and generalize this triplet-triplet annihilation research and its applications, making it more accessible by utilizing automated workflow systems as part of the latest NSF-powered Centre for Accelerated Photocatalysis (CAPs). She enjoys reading, journalling, and traveling to lakes and beaches in her free time. She's a big believer in retail therapy and is forever fascinated by people and their stories.

ACKNOWLEDGMENTS

First and foremost, I'd like to thank my research advisor, *Professor Phil Castellano*. I am indebted to him for offering his kind support and immaculate guidance and for instilling in me a sharp rigor and solution-oriented mindset that is invaluable not just for my professional but personal life. I am incredibly grateful to our DGP, *Professor Reza Ghiladi,* for his kind guidance, support, and untiring belief in me that has kept me sane throughout my graduate degree. I would also like to thank Professor *Elena Jakubikova* for making computational chemistry super fun and for her kind presence, which always wanted to make me do my best both in the classroom and in my research. I extend my heartiest gratitude to all my faculty for helping me become a well-rounded researcher and individual.

I want to thank my parents (*Rahat Shaheen* and *Muhammad Arshad Manzoor*), and my siblings (*Hafsa Arshad, Sania Arshad,* and *Hussain Arshad Khan*) for being my most significant support system, despite being on the other end of the world, not just during my graduate degree but throughout my life. I am so utterly grateful to them for enduring my stress-induced grumpiness and my inability to stay connected and give them the time they deserve because of being in different time zones. I thank them for calming me down and giving me the wings to soar higher in the pursuit of my dreams.

A special thank you to the Castellano group (present and past members), especially *Dr. Sam Shepard, Dr. Nancy Awwad, Dr. Evgeny Danilov,* and *Dr. Michael Rosko,* for training me and teaching me all the necessary skills and techniques crucial for my project.

I cannot end without mentioning some of my greatest inspirations and support in my peers and friends. Special thanks to Khawar Latif Khan, Shikufa Mousavi, Abdullah Irfan, Sultan Abdul

Wasay, Shehla Amir, Saad Shabeer, Zeinab Nizam, Heba Labib and Alissa Meo for sharing my passion, making me laugh during some of the most challenging times through this graduate journey, and providing some of the most insightful interdisciplinary ideas and approaches that helped me improve and polish my work.

TABLE OF CONTENTS

LIST OF TABLES

LIST OF SCHEMES

LIST OF FIGURES

Chapter 1: Fundamentals of Triplet-Triplet Annihilation Photon Upconversion (TTA-UC)

Photon upconversion refers to an anti-Stokes fluorescence process that has transformed and produced diverse cutting-edge applications. This phenomenon sums up energy from two low-energy photons within the incident light to create a single, high-energy photon of significantly greater energy.[1] The "anti-Stokes" designation refers to the striking blue-shift observed in the emission spectrum of the upconverted photon compared to the original absorption spectrum, defying the typical Stokes shift that characterizes conventional fluorescence processes.

As previously mentioned, photon upconversion has many applications, from oxygen sensing[1] and biological imaging[2] to photocatalyst systems[3], photovoltaics[4], and photochromic displays[5]. However, its most promising prospect lies in solar energy conversion. Upconverting sub-bandgap photons, an upconversion-equipped solar cell could potentially exceed the theoretical Shockley-Queisser efficiency limit of 33%[6] and achieve efficiencies higher than 43%.[7–9] Unfortunately, conventional upconversion systems relying on nonlinear phenomena, such as second-harmonic generation and two-photon absorption, require exceedingly high excitation power densities, typically in the range of megawatts to gigawatts per square centimeter, which is millions to billions of times greater than the power density of sunlight (around 100 milliwatts per square centimeter).[10–12] As a result, these approaches are impractical for photovoltaic applications. Fortunately, triplet-triplet annihilation-based upconversion has significantly lower power density requirements, enabling even non-coherent light sources like sunlight to trigger the upconversion process. This chapter will delve into the fundamental principles of triplet-triplet annihilation (TTA), a transformative development in the field of photon upconversion. We will explore the underlying mechanisms' details, the process's necessary requirements, and the associated kinetics.

A Brief History of TTA in Solution

In the pioneering work of the 1960s, Parker and Hatchard's discovery of upconverted fluorescence in donor/acceptor solutions (proflavine hydrochloride/anthracene or phenanthrene/naphthalene) marked a significant breakthrough in the field of TTA-sensitized upconversion.[13] However, this phenomenon remained largely unexplored in the following decades due to the inherent limitations of using organic chromophores as triplet photosensitizers - their low intersystem crossing (ISC) yields severely constrained the overall upconversion efficiency. It was not until the early 2000s that researchers[10,14–17] achieved a substantial advancement in this field by shifting their focus from organic molecules to the incorporation of metal-organic chromophores, such as ruthenium ($[Ru(dmb)_3]^{2+}$[4,4′-dimethyl-2,2′-bipyridine]ruthenium(II) $[Ru(dmb)_3]^{2+}$)[18], iridium (*tris*[2-phenylpyridinato-C2,N]iridium(III) $Ir(ppy)_3$)[19], zinc (ZnTPP)[20], platinum (PtTPBP[21], PtOEP[22]), and palladium (PdOEP[23], PdPh4TBP[24]) metalloporphyrin complexes, which exhibit remarkably higher efficiencies in generating the triplet state of the photosensitizer, paving the way for significant improvements in upconversion performance.

Mechanistic Overview

TTA involves a multi-step process, beginning with photosensitizer molecules in their ground state. First, a photosensitizer absorbs a photon and is promoted to an electronically excited singlet state. The excited photosensitizer then undergoes ISC, transitioning to the lowest excited triplet state. Next, this triplet-excited photosensitizer transfers its energy to an energetically appropriate acceptor/annihilator chromophore, thereby producing the triplet excited state of the acceptor. When two triplet-excited acceptor molecules interact, they can undergo triplet-triplet annihilation, resulting in one acceptor molecule in the excited singlet state and another in the ground state.

Finally, the singlet-excited acceptor relaxes to the ground state through radiative decay, emitting a higher energy than the initially absorbed photons. This connected sequence of energy transfer and conversion processes is illustrated in the Jablonski diagram presented in Scheme 1.1, which depicts the relative energy levels of the participating excited states in this TTA-based upconversion mechanism.

Scheme 0.1 Qualitative Jablonski Diagram Illustrating Heteromolecular Sensitized TTA-Based Upconversion.[a]

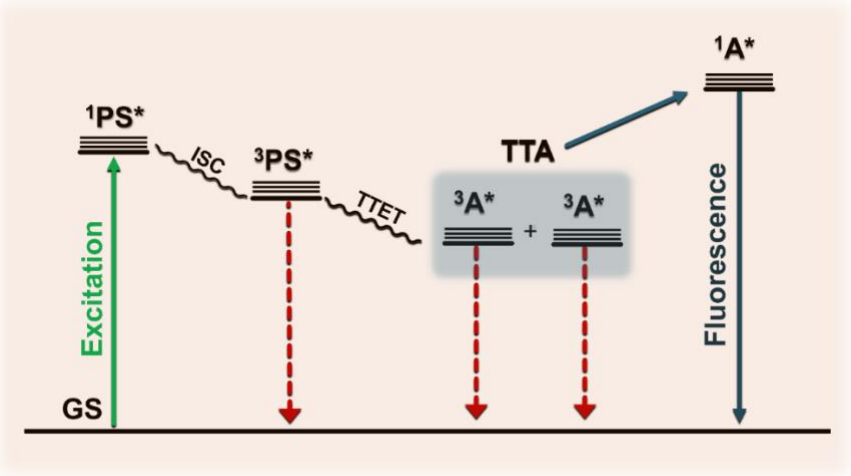

[a]GS = ground state, PS = photosensitizer, ISC = intersystem crossing, TTET = triplet−triplet energy transfer, A = acceptor/annihilator, TTA = triplet−triplet annihilation.

Criteria for Successful TTA-UC

Nature of the Molecules

For a molecule to be considered a suitable photosensitizer or acceptor/annihilator, it must meet specific criteria. To ensure effective photosensitization, the molecule must be a strong light absorber, with a large molar extinction coefficient in the visible or near-IR region. This allows it to efficiently absorb a significant amount of incident light, which is responsible for promoting the molecule to its excited singlet state. Correspondingly, the acceptor molecule should be a strong

emitter of light, exhibiting a high fluorescence quantum yield when emitting from its excited singlet state.

Beyond these absorption and emission properties, the pairing of the photosensitizer and acceptor molecules is crucial. The triplet energy level of the photosensitizer must be higher than that of the acceptor ($E_{triplet\ acceptor} \leq E_{triplet\ photosensitizer}$), enabling an efficient triplet-triplet energy transfer (TTET) process. The larger this energy difference, the more favorable the TTET will be, although this comes at the expense of a reduced anti-Stokes shift.[5]

The final key process is the annihilation itself. For this to be successful, the energy of the acceptor's excited singlet state must either be equal to or exceed the combined energy of two triplet-excited acceptor molecules ($E_{singlet\ acceptor} \leq 2E_{triplet\ acceptor}$). This larger driving force will favor the TTA process, even if it reduces the overall anti-Stokes shift.

Intersystem Crossing

Now that we have established the relative energetic requirements for the excited states involved in TTA, we must carefully examine the criteria necessary to efficiently convert the photosensitizer's excited singlet state to its triplet state. The process governing this critical conversion from singlet to triplet is known as intersystem crossing (ISC), a spin-forbidden process. However, this conversion is made possible through spin-orbit coupling, a fundamental concept that we must understand to optimize the efficiency of this crucial step in the TTA mechanism.

$$H_{SO} = -\frac{Z^4 e^2}{8\pi\varepsilon_0 m_e^2 c^2} l \cdot s \qquad \textbf{eq 1.1}$$

Eq 1.1[25] provides a simplified Hamiltonian expression that mathematically defines the spin-orbit coupling phenomenon. The variables involved include the atomic number of the nucleus (Z), the

elementary charge of the electron (e), the permittivity of the vacuum (ε_0), the mass of the electron (m_e), the speed of light (c), the orbital angular momentum (l), and the spin angular momentum (s). This equation is composed of two primary components: the vector component ($l \cdot s$), which represents the dot product of the orbital angular momentum and spin angular momentum, and the coefficients component ($\frac{Z^4 e^2}{8\pi\varepsilon_0 m_e^2 c^2}$), which is a collection of constants. In simple terms, the spin orbit coupling is an interaction between an electron's spin and its motion around the nucleus. This interaction results in a change in the electron's spin angular momentum, which is accompanied by a compensating change in its orbital angular momentum. Careful examination of eq 1.1 also reveals a direct proportionality between Z^4 indicates a crucial phenomenon: nuclei with higher atomic numbers exhibit stronger spin-orbit coupling, significantly enhancing singlet-triplet ISC efficiency. This effect is aptly termed the "heavy atom effect." Remarkably, the heavy nucleus and allows its larger and partially filled d-orbitals to interact with the excited molecules' orbitals, effectively driving the ISC efficiency towards near-unity levels.[26] This synergy is particularly evident when transition metals like zinc, palladium, and platinum, or larger halogen atoms such as iodine, bromine, and chlorine, are incorporated into porphyrins, phthalocyanines, or other transition metal complexes.[27,28]

Triplet-Triplet Energy Transfer: Dexter-Type Energy Transfer

Two types of triplet-triplet energy transfer occur within the TTA scheme. The first involves energy transfer from the photosensitizer's triplet state to the acceptor's triplet state. The second occurs between the triplet states of two acceptors, leading to annihilation. These energy transfer processes follow a Dexter-type energy transfer mechanism (Scheme 1.2).

Scheme 0.2 Schematic Representation of Dexter-Type Energy Transfer Mechanism.

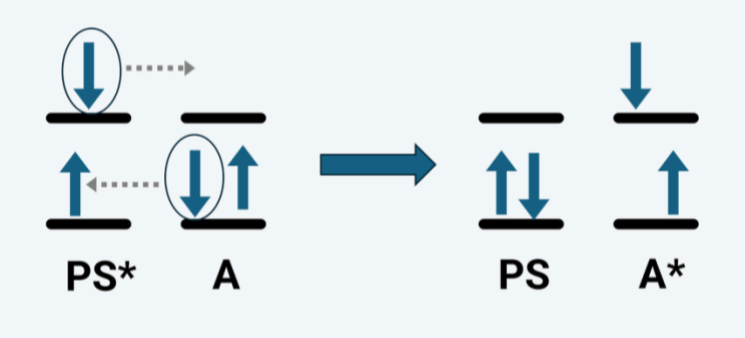

The Dexter energy transfer mechanism involves direct electron exchange between an excited photosensitizer molecule and an acceptor molecule. This charge transfer process causes the photosensitizer to become positively charged and the acceptor to be negatively charged. Subsequently, an electron is transferred back from the acceptor to the photosensitizer, leaving the acceptor in an excited state.[29] For this electron exchange to occur, the molecular orbitals of the photosensitizer and acceptor must overlap.[30] This spatial requirement limits Dexter transfer to a short-range, diffusion-controlled process that requires the photosensitizer and acceptor to be close to the range associated with Förster energy transfer.[30] Dexter energy transfer can occur efficiently even with minimal spectral overlap between the photosensitizer and acceptor. Notably, the overall spin of the system is preserved during this process, enabling both singlet-singlet and triplet-triplet energy transfer.

$$k_{ET} = KJ^{D}\exp\left(-\frac{2R}{L}\right) \qquad \textbf{eq 1.2}$$

$$K = \left(\frac{2\pi}{\hbar}\right)\kappa^{2} \qquad \textbf{eq 1.3}$$

$$J^{D} = \frac{\int f_{s}(\tilde{\nu})\varepsilon_{A}(\tilde{\nu})d\tilde{\nu}}{\int f_{s}(\tilde{\nu})d(\tilde{\nu})d\tilde{\nu}\int \varepsilon_{A}(\tilde{\nu})d\tilde{\nu}} \qquad \textbf{eq 1.4}$$

The rate of Dexter energy transfer (k_{ET}) is governed by an exponential relationship with the distance between the photosensitizer and acceptor molecules, as described by eq 1.2.[31] This equation incorporates parameters such as the effective average Bohr radius of the photosensitizer and acceptor (L), K is a the constant defined in eq 1.3 (where κ is another constant with energy units). The Dexter overlap integral (J^D), as described by eq 1.4, which is calculated from the absorption spectrum of the acceptor (ε_A) and the fluorescence spectrum of the photosensitizer (f_s), across the relevant wavenumber range ($\tilde{\upsilon}$).[31–33] Understanding this Dexter energy transfer process is crucial for optimizing and improving the efficiency of various photophysical and photochemical applications utilizing TTA.

Spin Statistics

It is established that the TTA process can generate higher excited spin allowed species. While Nickel[33] demonstrated that the annihilation event produces the highest energetically accessible singlet state product, early work suggested that TTA's efficiency is limited by spin statistics - the singlet is just one of several possible outcomes.[34–38] This is because the number of possible encounter-pair spin states equals the product of the spin multiplicities of the combining species. With each acceptor triplet ($^3A_1^*$) having a spin multiplicity of 3, there are 9 possible sub-states. Applying spin quantum number rules which state that S (M = 2S +1), these 9 sub-states can be singlet - $^1(^3A_1{}^3A_1)$, triplet - $^3(^3A_1{}^3A_1)$, or quintet - $^5(^3A_1{}^3A_1)$, all with equal probability. Considering the multiplicity of these spin states, 5 are quintet, 3 are triplet, and 1 is singlet, as shown in the eq 1.5 – 1.7.[39]

$$^3A_1^* + {}^3A_1^* \leftrightarrow {}^5(AA)_2^* \leftrightarrow {}^5A_2^* + {}^1A_0 \qquad \textbf{eq 1.5}$$

$$^3A_1^* + {}^3A_1^* \leftrightarrow {}^3(AA)_1^* \leftrightarrow {}^3A_2^* + {}^1A_0 \qquad \textbf{eq 1.6}$$

$$^3A_1^* + {}^3A_1^* \leftrightarrow {}^1(AA)_0^* \leftrightarrow {}^1A_2^* + {}^1A_0 \qquad \textbf{eq 1.7}$$

Based on the Wigner Spin Rules,[65] the probability of an annihilation event producing an excited singlet molecule should be only 11.1% (one of the nine possibilities).[34–38] Yet, TTA processes often exhibit quantum efficiencies exceeding 40%[28,40] - much higher than the statistical limit. This discrepancy can be explained by the fate of the triplet and quintet encounter complexes formed during the TTA process. The excited quintet state typically has very high energy, so the energy available from the annihilating triplets is insufficient to create an excited quintet molecule.[36,37] Instead, the quintet encounter complex will likely decay into two triplet excited states. Similarly, the $^3A_2^*$ state is often inaccessible given the available energy, so the triplet encounter complex would dissociate into two $^3A_1^*$ states, which can then participate in the next annihilation event. This way, the quintet and triplet encounter complexes are effectively recycled back into triplet states,[40,41] leading to enhanced TTA quantum efficiency.

The Relationship Between Delayed Fluorescence and TTA

After the photosensitizer is excited by long-wavelength light, efficient absorption of photons follows, leading to ISC and triplet-triplet energy transfer. This culminates in the final step of the TTA process, where the excited singlet of the acceptor is created and then fluoresces. This fluorescence, resulting from the final step of TTA, is termed "delayed fluorescence." This phenomenon was first observed in solutions of aromatic carbon compounds in the early 1960s.[13,42–44] Delayed fluorescence can be divided into two classes: pyrene-type (P-type) and eosin-type (E-type), although only the P-type is relevant to sensitized photochemical upconversion.[43] Both of these types are depicted in Scheme 1.3.

Scheme 0.3 Jablonski Diagram of E-Type and P-Type Delayed Fluorescence.

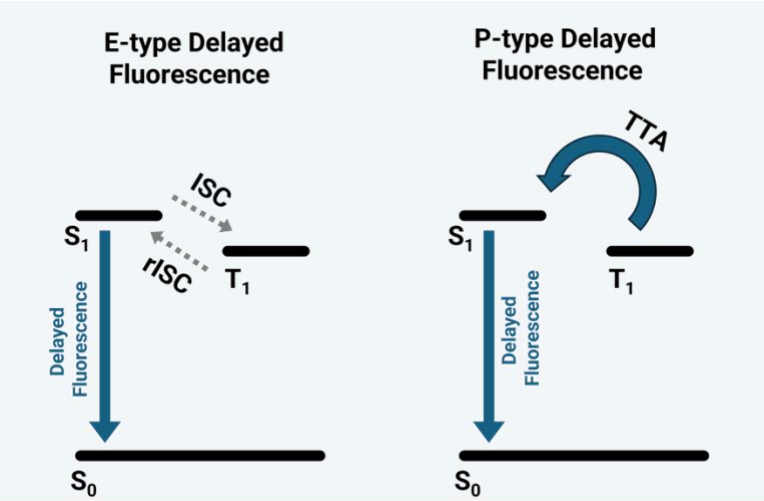

The P-type delayed fluorescence was first discovered in solutions of pyrene and phenanthrene, hence the name. This type of delayed fluorescence has an intensity proportional to the square of the rate of absorption of the exciting light, and it is attributed to the formation of excited dimers created by the combination of two molecules in the triplet state.[43,44] One of these excited dimers then emits or decays, producing an excited singlet molecule and an unexcited molecule. This process occurs in aromatic hydrocarbons where the energy gap between the singlet fluorescent state (S_1) and the low-lying triplet state (T_1) is sufficiently large, preventing thermal activation to the excited singlet state at room temperature.[39] Pyrene-type delayed fluorescence can be distinguished experimentally from the eosin-type, which is produced by thermal activation of the first excited triplet state to the first excited singlet state. The eosin-type delayed fluorescence only occurs when the energy gap between the singlet and triplet states is small enough to allow thermal repopulation of the excited singlet state from the triplet state via reverse intersystem crossing (rISC).[45]

Collision-Induced Kinetics of Triplet-Triplet Annihilation

Cutting-edge research has unveiled the immense potential of UC-TTA in revolutionizing solar energy, photocatalysis, biological imaging, and photochemical drug activation. Yet, the critical role of chemical kinetics in optimizing upconversion efficiency remains largely underexplored. This section discusses how reaction kinetics are the driving force behind photochemical upconversion and are crucial to optimizing the strategic design of both established and novel upconversion systems.

Before discussing collisional quenching, we must first understand the concept of quenching. Quenching refers to decreased photoluminescence intensity through various processes, such as excited-state reactions, molecular rearrangements, energy transfer, ground-state complex formation, and collisional quenching.[29] This section will focus on bimolecular collisional quenching, as it is central to the TTET within the TTA mechanism. During collisional quenching, an excited-state fluorophore collides with a quencher molecule via diffusion, which occurs within the excited-state species' lifetime. As a result of this contact, the excited-state species non-radiatively returns to its ground state.

$$\frac{I_0}{I} = \frac{\tau_0}{\tau} = 1 + k_q\tau_0[Q] = 1 + K_{SV}[Q] \qquad \textbf{eq 1.8}$$

$$K_{SV} = k_q\tau_0 \qquad \textbf{eq 1.9}$$

The mathematical description of this collisional quenching is given by the Stern-Volmer relationship presented in eq 1.8 and where I_0 and I are the photoluminescence intensities in the absence and presence of quencher respectively, k_q is the bimolecular quenching rate constant, τ_0

is the lifetime of excited state fluorophore in the absence of quencher; [Q] is the concentration of the quencher molecule; K_{SV} is the Stern-Volmer constant defined by eq 1.9.

It is important to note that eq 1.8 does not apply to static quenching. During static quenching, a non-fluorescent complex forms between the fluorophore and quencher. Hence, there is no decrease in the measured photoluminescence lifetime – only photoluminescent molecules (uncomplexed) that retain the unquenched lifetime (τ_0) can be observed. Dynamic Stern-Volmer plots present the ratio of $\frac{I_0}{I}$ or $\frac{\tau_0}{\tau}$ as a function of quencher concentration, which is expected to be linearly dependent, as shown in Figure 1.1. The slope of a Stern-Volmer plot represents K_{sv}, which allows determination of the quenching rate constant k_q if the excited state photosensitizer lifetime (τ_0), is known.

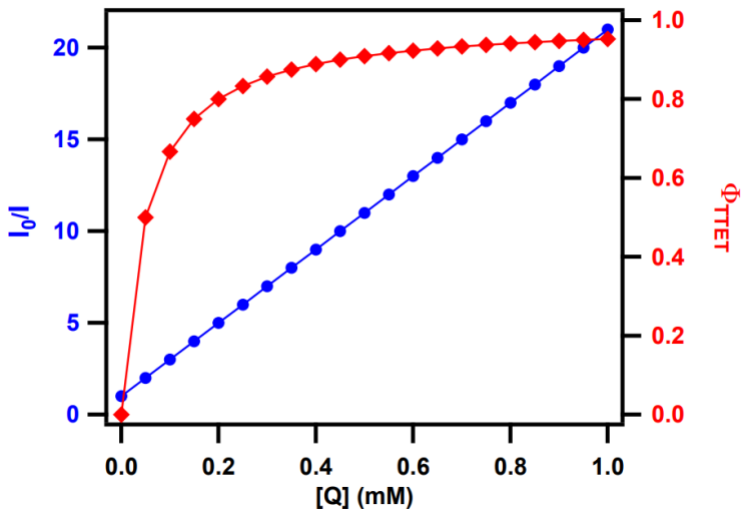

Figure 0.1 Stern-Volmer plot (in blue dotted points) and triplet-triplet energy transfer efficiency plot (in red diamond points) for quenching of a hypothetical photosensitizer with an unquenched lifetime of 20 µs. A linear

Stern-Volmer plot yields an intercept of 1 on the y-axis and a slope equal to the Stern-Volmer constant K_{sv} = 2.0×10^4 M^{-1}, giving $k_{TTET} = 1.0 \times 10^9$ $M^{-1}s^{-1}$ ($K_{sv} = k_{TTET}t_0$).[46]

As mentioned earlier, TTET occurs through a diffusion-controlled Dexter mechanism, which can be viewed as a photosensitizer quenching process resulting from the direct collision between the donor and acceptor.[47] Consequently, when the photosensitizer decays through first-order kinetics, the quenching rate constant, k_q, is equivalent to the triplet energy transfer rate constant (k_{TTET}) which further enables us to use the Stern-Volmer equation to estimate the triplet-energy transfer efficiency (Φ_{TTET}) using eq 1.10. Careful examination of the equation reveals that maximizing the efficiency of this process necessitates that all photosensitizer-excited triplet states be effectively quenched by acceptor molecules, yielding excited triplet acceptors.[47] Crucially, the system must not contain any other species capable of interacting with these triplets, particularly ground state dioxygen. This is because the quenching of the photosensitizer triplet state is a second-order bimolecular reaction, where the rate constant k_{TTET} is ultimately limited by the diffusion-controlled rate constant k_d. The diffusion-controlled rate constant k_d can be estimated using eq 1.11, which incorporates the gas constant (R), temperature (T), and solvent viscosity (η). If quenching is diffusion-controlled, k_q is approximately equivalent to k_d.[48] It is important to note that the diffusion-controlled rate constant, k_d, depends solely on the properties of the solvent without incorporating any molecular parameters associated with the reacting species.

$$\Phi_{TTET} = \left(1 - \frac{I}{I_0}\right) - \left(1 - \frac{\tau}{\tau_0}\right) = \frac{k_{TTET}\tau_0[Q]}{1+k_{TTET}\tau_0[Q]} \qquad \textbf{eq 1.10}$$

$$k_d = \frac{8RT}{3\eta} \qquad \textbf{eq 1.11}$$

The diffusion-limited rate constant in the solvent provides a valuable reference point for researchers to compare measured k_{TTET} and assess performance targets. Effective TTET requires

the overall TTET rate to be valued at least two orders of magnitude higher than the triplet decay.[47] The TTET efficiency can be increased by raising the quenching rate constant (k_q), extending the triplet lifetime, or increasing the quencher concentration, often the latter being the most readily adjustable parameter. For instance, a 1 mPa·s solvent viscosity corresponds to a diffusion-controlled k_d of 7×10^9 $M^{-1}s^{-1}$. Assuming a diffusion-controlled k_{TTET} of 1×10^9 $M^{-1}s^{-1}$ and a 10 μs triplet lifetime, a quencher concentration of 0.1 mM can make quenching competitive with the inherent photosensitizer lifetime. Efficient TTET is generally challenging for photosensitizers with lifetimes shorter than 1 μs, whereas those with longer excited-state lifetimes are more suitable for triplet energy transfer.[47]

After the occurrence of TTET, the sensitized triplet states would decay via two competing deactivation pathways - parallel first-order and second-order decay processes. The kinetics for these decay processes are represented by eq 1.12.

$$\frac{d[^3A^*]_t}{dt} = -k_T[^3A^*]_t - k_{TT}[^3A^*]_t^2 \qquad \textbf{eq 1.12}$$

$$\frac{[^3A^*]_t}{[^3A^*]_0} = \frac{1-\beta}{e^{k_T t}-\beta} \qquad \textbf{eq 1.13}$$

$$\beta = \frac{k_{TT}[^3A^*]_0}{k_T + k_{TT}[^3A^*]_0} \qquad \textbf{eq 1.14}$$

$$\Delta A = \frac{\Delta A_0(1-\beta)}{e^{k_T t}-\beta} \qquad \textbf{eq 1.15}$$

The first-order decay term ($k_T[^3A^*]_t$) encompasses both the inherent triplet-state decay of the acceptor/annihilator and the pseudo-first-order quenching by dioxygen and other species. The second-order component ($k_{TT}[^3A^*]_t^2$) represents the bimolecular triplet quenching via the TTA process. This competition between the two kinetic mechanisms leads to distinct kinetic regimes,

which will be discussed further in the Quadratic-to-Linear Power Dependence section. The analytical solution to eq 1.12 from Bachilo and Weisman, as presented in eq 1.13,[36] features a dimensionless parameter β that ranges from 0 to 1 and corresponds to the initial fraction of decay occurring through the second-order TTA channel. In some literature, α is used to denote the product of the TTA rate and the initial concentration of the acceptor/annihilator triplets ($\alpha = k_{TT}[^3A^*]_0$ which leads to $\beta = \frac{\alpha}{k_T+\alpha}$). Eq 1.13 can be rewritten in terms of transient absorption kinetic parameters as eq 1.15. The initial concentration of acceptor/annihilator triplets ($[^3A^*]_0$) can be readily calculated if their extinction coefficient (ε_T) has been measured based on the triplet decay kinetics. This kinetic analysis has been heavily utilized to study the homomolecular triplet-triplet annihilation (HTTA) in metalloporphyrins in Chapter 2 of this document.

The Transition from Quadratic-to-Linear Power Dependence

Measuring the dependence of photoluminescence intensity on the intensity of incident light is a standard method to investigate whether the observed photoluminescence arises from upconversion. This power dependency experiment is typically conducted using steady-state photoluminescence, employing a range of coherent or incoherent excitation sources that allow for scanning irradiance intensities across multiple orders of magnitude.[49] Figure 1.2 provides some reference data sets which will be used for further explanation.

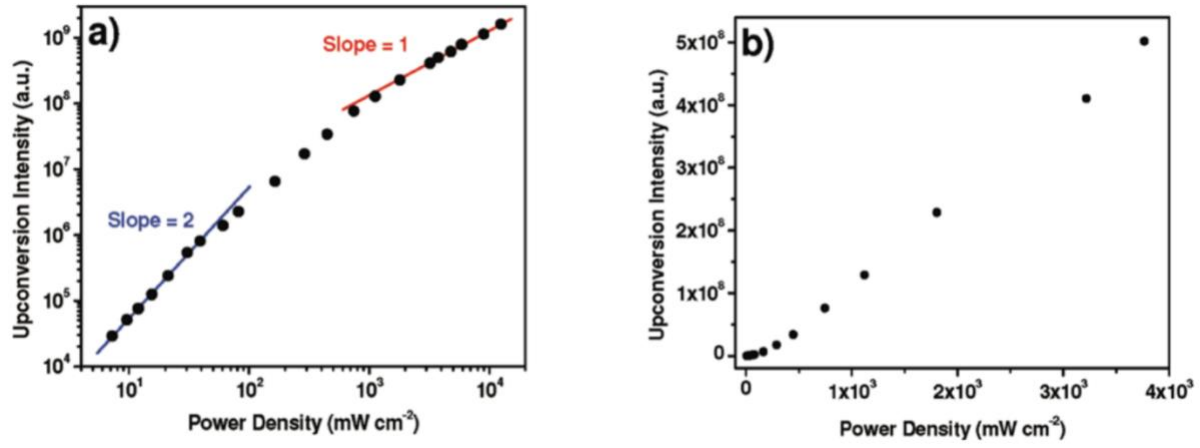

Figure 0.2 (a) Double logarithmic plot of the upconversion emission signal at 420 ± 6 nm measured as a function of 514.5 nm incident laser power in a mixture of PdOEP and DPA in argon-degassed toluene. The colored lines are the linear fits with slopes of 1.0 (red, linear response) and 2.0 (blue, quadratic response) in the high and low power regimes, respectively. (b) Linear plot of the first 19 data points presented in panel a. Figure was adapted from reference.[49]

At low excitation power, the upconverted photoluminescence shows a quadratic dependence on the incident light.[42] Here, the TTA-UC kinetics are governed by the first-order decay of acceptor/annihilator triplets. However, as the power exceeds a threshold represented as the I_{th}

point, the dependence transitions to a linear relationship.[40,50] Above this point, the increased excitation provides more triplets, allowing TTA to outcompete their first-order decay. Consequently, the upconverted fluorescence scales linearly with excitation in this strong annihilation regime. This is where the maximum possible quantum efficiency for the photosensitizer/annihilator pair is expected to occur.[49,50]

Eq 1.12 quantitatively reveals the divergence of the power dependence from quadratic to linear. Evaluating this equation pinpoints the two kinetic limits of the $^3A^*$ decay, as the associated upconverted fluorescence intensity (N_F) scales with the square of the $^3A^*$ population, as shown in eq 1.16[49] where Φ_F represents the fluorescence quantum yield of the acceptor/annihilator. Importantly, eq 1.13 and 1.14 identify the two competing kinetic processes: k_T – the unimolecular and pseudo-first-order decay pathway for the acceptor triplets – and k_{TT} – the second-order TTA of the acceptor triplets.[47,49]

$$N_F = \int_0^\infty I_F(t)dt = \int_0^\infty \Phi_F k_{TT}[^3A^*]_t^2 \qquad \textbf{eq 1.16}$$

$$[^3A^*]_t = [^3A^*]_0 e^{-k_T t} \qquad \textbf{eq 1.17}$$

$$N_F = \frac{\Phi_F k_{TT}[^3A^*]_0^2}{2k_T} \qquad \textbf{eq 1.18}$$

The governing equation (eq 1.13) simplifies to a single exponential decay when the triplet-triplet annihilation rate is significantly smaller than the triplet decay rate (eq 1.17) – weak annihilation limit. Once we substitute eq 1.17 into eq 1.16 and integrate it with respect to time, we get eq 1.18. This analysis demonstrates that the upconverted fluorescence exhibits a quadratic relationship, scaling proportionally with the square of the absorbed optical power, which is directly related to the excited triplet concentration.

$$[^3A^*]_t = \frac{[^3A^*]_0}{1+k_{TT}[^3A^*]_0 t} \qquad \textbf{eq 1.19}$$

$$N_F = \Phi_F[^3A^*]_0 \qquad \textbf{eq 1.20}$$

Conversely, when the triplet-triplet annihilation rate exceeds the first order triplet decay rate – strong annihilation limit, the eq 1.13 can be simplified to eq 1.19, and the integration over time for this equation gives us eq 1.20, indicating a linear proportionality between the total intensity of upconverted emission and the incident light power. This kinetic analysis aligns with the previous work on conventional delayed fluorescence by Birks and Parker over 50 years ago.[39,51]

Several key factors must be considered to maximize the efficiency of TTA upconversion. First, optimal upconversion quantum yields are anticipated in the strong annihilation regime, where the bimolecular TTA process no longer limits the rate compared to the first-order decay of acceptor triplets. Second, any energy-dissipating quenching processes of the annihilator triplets will diminish efficiency by hindering the TTA kinetics. Consequently, using degassed solvents or oxygen-impermeable host media is essential in upconversion experiments. Third, the photosensitizers' excitation wavelengths and optical densities should be optimized to reach the strong annihilation regime at the lowest possible optical power.[49] The upconversion quantum yield (Φ_{UC}) is a critical metric employed to evaluate the overall efficiency of each upconversion system. Detailed protocols for measuring photochemical upconversion quantum yields have been provided for those interested and can be accessed in a recent review article.[52]

Metalloporphyrins As Triplet Photosensitizers for TTA

Closed-shell metalloporphyrins are poised to revolutionize the realm of TTA processes. Firstly, TTA in these systems facilitates the formation of a highly luminescent excited singlet state,

perfectly resonant with twice the energy of the interacting triplet. This remarkable attribute minimizes energy losses, maximizing the efficiency of the upconverted singlet state. Specifically, the $2T_1 \rightarrow S_n + S_0$ process preferentially generates the excited singlet, where the energy gap between S_0 and T_1 precisely matches the gap between S_0 and S_n, and the $S_0 \rightarrow S_n$ radiative transition exhibits an exceptionally large oscillator strength.[33] This preferred product state aligns seamlessly with the one-photon excitation in their robust Soret bands, unlocking unparalleled synergies for closed-shell metalloporphyrins. Secondly, metalloporphyrins with d_0 or d_{10} electron configurations possess Soret-excited states with lifetimes in the picosecond range, rendering them highly efficient energy/electron donors in various materials.[19] Thirdly, as potential dual photosensitizers/emitters, ISC can form triplets with astounding yield and minimal thermal loss, with lifetimes spanning tens or even hundreds of microseconds.[35] Finally, the ability of metalloporphyrin derivatives to capture a vast fraction of the solar spectrum, displaying strong absorption well into the near-infrared, positions them as transformative alternatives to conventional dyes. Collectively, these exceptional characteristics make closed-shell metalloporphyrins a compelling and versatile platform for TTA applications.

Metalloporphyrins pose a formidable challenge in accurately measuring their photoluminescence from upper excited states. Their absorption and emission spectra heavily overlap, with minuscule Stokes shifts (few hundred wavenumbers between the maxima of their $S_0 \rightarrow S_2$ absorption and $S_2 \rightarrow S_0$ emission bands), leading to extensive reabsorption and distortion of fluorescence signals.[53] Compounding this, the intense Soret absorption ($\varepsilon_{max} \sim 5 \times 10^5$ M^{-1} cm^{-1}), and their upper excited states having fleeting lifetimes ($\leq 10^{-12}$ s) and very low quantum yields ($\leq 10^{-3}$), create further obstacles in obtaining undistorted spectra and reliable quantum yield measurements. Overcoming

these challenges requires the use of highly purified samples, powerful excitation sources, and meticulous mitigation of scattering and reabsorption effects.[53,54]

In the following chapter, we investigate the HTTA process occurring in widely utilized metalloporphyrin photosensitizers. Employing the robust technique of transient absorption spectroscopy, we circumvent the intricacies associated with fluorescence and quantum yields, enabling us to thoroughly examine the TTA dynamics and kinetics within these metal-based porphyrin systems. The following section provides a brief overview of the techniques utilized in this endeavor.

Experimental Techniques

Electronic Absorption Spectroscopy

Ultraviolet-visible spectroscopy is a technique employed to investigate the transitions associated with photon absorption within the ultraviolet and visible regions of the electromagnetic spectrum. By analyzing the light transmitted through a sample, or the transmittance across the UV-Vis spectrum, researchers can assess both the types and the intensity of these transitions as a function of wavelength from the collected data. There are two primary types of monochromator UV-Vis spectrophotometers: single beam and dual beam, as depicted in the Figure 1.3.[55]

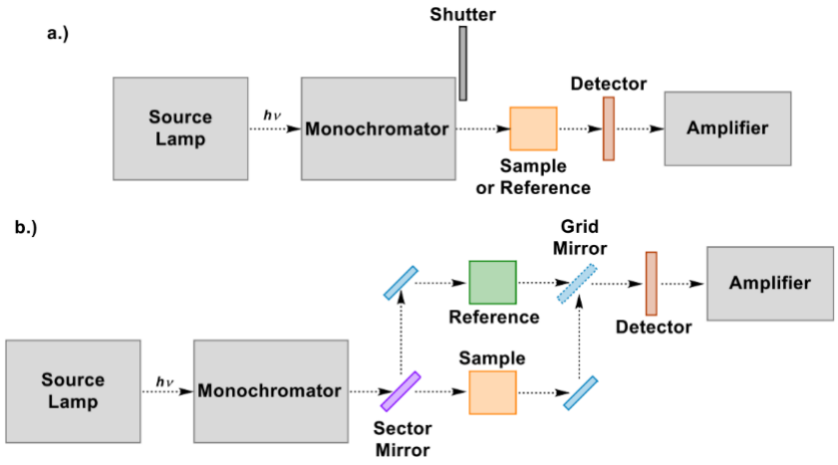

Figure 0.3 Schematics for typical single beam (a) and double beam (b) UV-Vis spectrophotometers.[64]

In a single-beam instrument, measurements initially require the subtraction of a solvent blank from the background, after which the sample can be recorded. Conversely, unlike the single beam setup, a dual beam instrument can simultaneously record the solvent blank reference and the sample. Using two beam paths in the dual-beam design enables faster data acquisition and more reproducible experiments, though this instrumentation is more expensive than the single-beam equipment.[56] Schematics of UV-Vis spectrophotometers invariably encompass three indispensable components: a versatile light source, a precision monochromator, and a sensitive detector. The light source can be tailored to the required wavelengths, offering options such as deuterium/hydrogen, tungsten filament, and xenon lamps.[55] The monochromator meticulously takes the light generated from the source and separates it into discrete wavelengths using a sophisticated diffraction grating. Many commercially available UV-Vis spectrophotometers employ the renowned Czerny-Turner configuration, where the light enters the monochromator through the entrance slit, reflects off a concave collimating mirror onto a reflection grating, which then disperses the white light into its components.[57,58] By precisely adjusting the angle of reflection off the diffraction grating, the desired wavelengths can be selectively deflected off a second

concave mirror and pass through the exit slit. Detectors can be classified as either scanning, such as photomultiplier tubes and photodiodes, or non-scanning, like photodiode arrays and charge-coupled device cameras.[55] Non-scanning detectors can capture all light simultaneously, allowing the diffraction grating to remain stationary in devices equipped with such advanced detectors.[55]

$$T = \frac{I}{I_0} \qquad \textbf{eq 1.21}$$

$$A = -\log(T) \qquad \textbf{eq 1.22}$$

$$A = \varepsilon bc \qquad \textbf{eq 1.23}$$

Acquiring the absorption spectrum of a sample begins with measuring the transmittance (T) as depicted in eq 1.21. This equation utilizes the ratio of light intensity transmitted (I) through the sample relative to the reference (I_0). The relationship between absorbance and transmittance is described by eq 1.22. Additionally, the absorbance of a sample can be correlated to its concentration at a specific wavelength using the Beer-Lambert Law[59,60], as stated in eq 1.23. Absorbance, a dimensionless quantity, depends on the sample's pathlength (b, measured in cm) and molar absorptivity (ε, M^{-1} cm^{-1}), which varies with the sample and the wavelength of light. Sample absorptivity typically exhibits a linear trend at spectroscopic scale concentrations. However, at high concentrations, solvent-solute, solute-solute, or hydrogen bonding interactions may influence the analyte environment, causing deviations from the Beer-Lambert law.[55,60] Measurements are often performed at dilute concentrations, typically much less than 0.01 M, to account for these deviations.

Transient Absorption Spectroscopy

Transient absorption spectroscopy, a time-resolved technique, enables observing absorption profiles and decay kinetics of excited state species. This method operates on the principles of pump-probe spectroscopy, which requires two light sources. The "pump" beam, a timed laser pulse, excites a fraction of the molecules in the solution at a particular wavelength, promoting them to an electronically excited state. The "probe" beam is then utilized to monitor the absorption profile of the photoproduct. Transient species can be studied using two types of transient absorption methods: femtosecond TA and nanosecond TA. Femtosecond TA, commonly termed ultrafast TA, can detect events occurring on short timescales from hundreds of femtoseconds to thousands of picoseconds. Alternatively, nanosecond TA can measure events taking place from and beyond tens of nanoseconds.

$$\Delta A = A(t) - A_0 = \varepsilon^* b[S^*] - \varepsilon b[S^*] - (\varepsilon^* - \varepsilon) b[S^*] \qquad \textbf{eq 1.24}$$

$$\Delta A = -\log\left(\frac{T(t)}{T_0}\right) \qquad \textbf{eq 1.25}$$

Transient absorption spectroscopy leverages the insights gained from eq 1.24 and 1.25 to precisely measure the change in absorption between the excited state and ground state species.[60,61] Extending the Beer-Lambert law, this technique can observe the fleeting absorbance of transient species. The change in absorbance, ΔA, dramatically contrasts the pre-pulse, A_0, and post-pulse, A(t), measurements. Crucially, the distinct electronic signatures of ground and excited state molecules, encoded in their respective extinction coefficients, ε and ε^*, and the concentration of the excited state $[S^*]$, enable quantifying the change in excited state absorption after the laser pulse. These parameters are extracted by probing the transmittance before, T_0, and after, T(t), the laser pulse.

The change in absorbance can manifest as either positive or negative features. A "ground state bleach," a negative feature, indicates that a fraction of the ground state species was promoted to the excited state. Conversely, positive features reveal the presence of an observable excited state following excitation. Intuitively, a bleach signal permits more photons of a given wavelength to reach the detector, while an excited state feature blocks more photons compared to the ground state molecule.

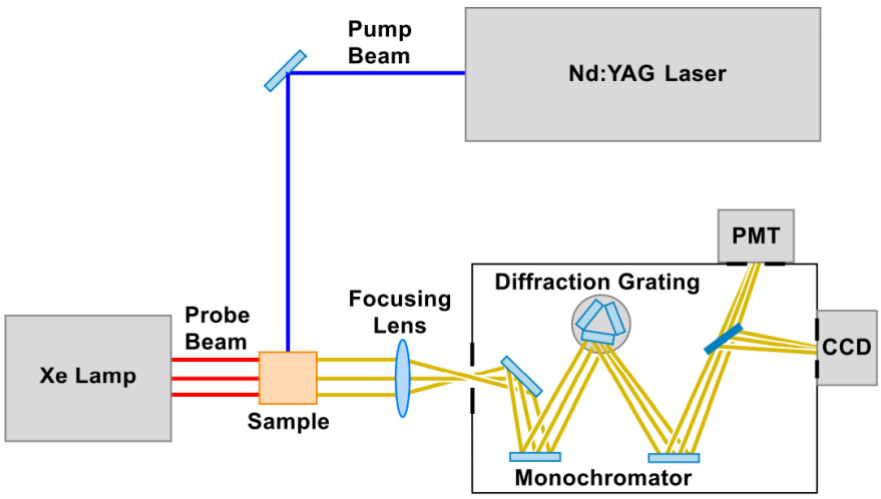

Figure 0.4 Box diagram of nanosecond transient absorption apparatus. [64]

Researchers can use a nanosecond transient absorption (nsTA) apparatus to probe photoexcited molecules across various timescales, from tens of nanoseconds to hundreds of milliseconds. The nsTA setup in our laboratory, as depicted in Figure 1.4, employs a tunable Nd:YAG/OPO laser (Opotek Radiant QX4130 tunable laser system) to provide the pump excitation beam, which is directed into the sample chamber. Samples are then probed with intense white light pulses generated by a Xe arc lamp, positioned perpendicular to the excitation pulse. Proper experimental conditions necessitate the spatial overlap of the pump and probe beams onto the sample, enabling the observation of excited state absorption. The temporal overlap of the pump and probe

determines the time-zero reference. Optical filters, such as long-pass and neutral density filters, may be strategically placed around the sample to block laser scatter or protect the sample from photodegradation. Within the instrument, a monochromator disperses the light, which is then directed into either an iStar CCD camera (Andor Technologies) for spectral measurements or an R2658P PMT (Hamamatsu) detector. The instrument's time resolution is electronically controlled through the L900 software interface.

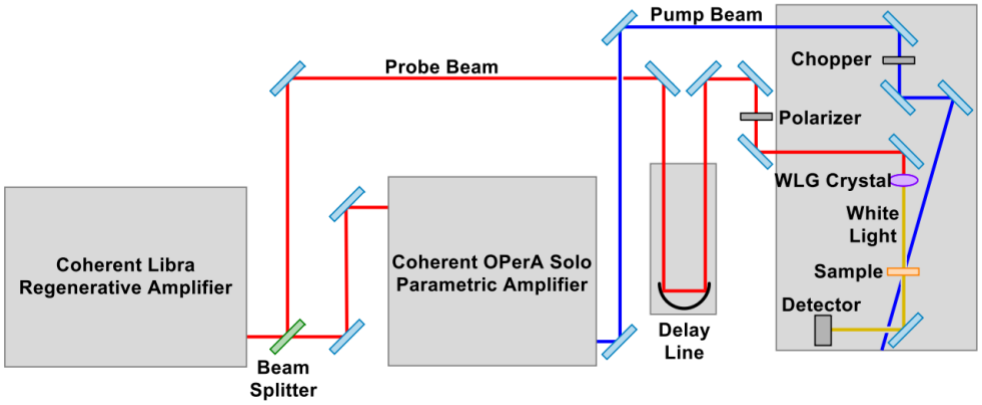

Figure 0.5 Box diagram of ultrafast transient absorption apparatus.[64]

Events too brief to be captured by conventional nsTA instrumentation, can be detected in the UFTA instrumentation. The schematic of our UFTA setup is depicted in the accompanying Figure 1.5. Precise spatial and temporal overlap of the pump and probe beams is crucial for accurately obtaining the time-zero point and recording the difference spectra and kinetics. A Ti:Sapphire Coherent Libra regenerative amplifier generates a high-energy, 1 kHz, 800 nm pulsed beam, which is divided into the probe and pump beams. The probe beam is directed to an optical delay stage, enabling precise control of the time delay between 0 and 6 ns. By leveraging the speed of light, the pulses at a range of time delays can be measured as the delay line extends the distance the probe beam must travel. The probe beam then passes through a polarizer positioned at the magic

angle (54.7°) to eliminate potential artifacts.[62] Depending on the desired white light continuum, either a CaF_2 (provides a range of 330 – 750 nm) or a sapphire crystal (offers a range of 450 – 750 nm) can generate the probe beam in the UV-vis or visible spectrum, respectively.[63] Due to their thermal instability, CaF_2 crystals are mounted on a continuously moving translational stage for protection.[63] Concurrently, the pump beam enters a Coherent OPerA Solo parametric amplifier to produce a tunable excitation. The pump beam is then directed through a 500 Hz optical chopper, which blocks every other pulse from the pump, enabling consecutive measurements with and without excitation to calculate the absorbance change.[63] The pump and probe beams overlap and interact in the sample, which is housed in a 2 mm quartz cuvette, to detect the transient species which are then detected through a fiber optic cable.

Conclusion

This chapter introduced the fundamental concepts of triplet-triplet annihilation photon upconversion, a process that holds immense potential for various applications, most notably in solar energy conversion. We delved into the mechanics of this anti-Stokes fluorescence process, where two low-energy photons combine their energy to generate a single, higher-energy photon. A key highlight of this chapter was distinguishing TTA-UC from traditional upconversion methods. Unlike its counterparts that rely on high excitation power densities, TTA-UC operates efficiently even with readily available, non-coherent light sources like sunlight. This unique advantage stems from the lower power density requirements of the TTA mechanism, a process we explored in detail, including its dependence on factors like delayed fluorescence and collision-induced kinetics. Furthering our understanding of TTA-UC, we discussed the experimental techniques employed to study and characterize this phenomenon. The relationship between delayed fluorescence and TTA was highlighted, emphasizing its role in elucidating the kinetics

and efficiency of the upconversion process. Singh-Rachford and Castellano provided a comprehensive examination of TTA-UC with their review article[10], and this chapter serves as a foundation for understanding its intricacies. The subsequent chapter will detail my research and experimentation studying TTA in homomolecular metalloporphyrins.

References

(1) Zhang, P.; Steelant, W.; Kumar, M.; Scholfield, M. Versatile Photosensitizers for Photodynamic Therapy at Infrared Excitation. *J. Am. Chem. Soc.* **2007**, *129* (15), 4526–4527.

(2) Liu, Q.; Yang, T.; Feng, W.; Li, F. Blue-Emissive Upconversion Nanoparticles for Low-Power-Excited Bioimaging in Vivo. *J. Am. Chem. Soc.* **2012**, *134* (11), 5390–5397.

(3) Zhang, Z.; Wang, W.; Yin, W.; Shang, M.; Wang, L.; Sun, S. Inducing Photocatalysis by Visible Light beyond the Absorption Edge: Effect of Upconversion Agent on the Photocatalytic Activity of Bi2WO6. *Appl. Catal. B Environ.* **2010**, *101* (1–2), 68–73.

(4) Singh-Rachford, T. N.; Lott, J.; Weder, C.; Castellano, F. N. Influence of Temperature on Low-Power Upconversion in Rubbery Polymer Blends. *J. Am. Chem. Soc.* **2009**, *131* (33), 12007–12014.

(5) Miteva, T.; Yakutkin, V.; Nelles, G.; Baluschev, S. Annihilation Assisted Upconversion: All-Organic, Flexible and Transparent Multicolour Display. *New J. Phys.* **2008**, *10* (10), 103002.

(6) Shockley, W.; Queisser, H. J. Detailed Balance Limit of Efficiency of P-n Junction Solar Cells. *J. Appl. Phys.* **1961**, *32* (3), 510–519.

(7) Tayebjee, M. J.; McCamey, D. R.; Schmidt, T. W. Beyond Shockley–Queisser: Molecular Approaches to High-Efficiency Photovoltaics. *J. Phys. Chem. Lett.* **2015**, *6* (12), 2367–2378.

(8) Trupke, T.; Green, M.; Würfel, P. Improving Solar Cell Efficiencies by Up-Conversion of Sub-Band-Gap Light. *J. Appl. Phys.* **2002**, *92* (7), 4117–4122.

(9) Cheng, Y. Y.; Nattestad, A.; Schulze, T. F.; MacQueen, R. W.; Fückel, B.; Lips, K.; Wallace, G. G.; Khoury, T.; Crossley, M. J.; Schmidt, T. W. Increased Upconversion Performance for Thin Film Solar Cells: A Trimolecular Composition. *Chem. Sci.* **2016**, *7* (1), 559–568.

(10) Singh-Rachford, T. N.; Castellano, F. N. Photon Upconversion Based on Sensitized Triplet–Triplet Annihilation. *Coord. Chem. Rev.* **2010**, *254* (21), 2560–2573.

(11) Monguzzi, A.; Tubino, R.; Hoseinkhani, S.; Campione, M.; Meinardi, F. Low Power, Non-Coherent Sensitized Photon up-Conversion: Modelling and Perspectives. *Phys. Chem. Chem. Phys.* **2012**, *14* (13), 4322–4332.

(12) Islangulov, R. R.; Castellano, F. N. Photochemical Upconversion: Anthracene Dimerization Sensitized to Visible Light by a RuII Chromophore. *Angew. Chem.* **2006**, *118* (36), 6103–6105.

(13) Parker, C. A.; Hatchard, C. G. Delayed Fluorescence from Solutions of Anthracene and Phenanthrene. *Proc. R. Soc. Lond. Ser. Math. Phys. Sci.* **1962**, *269* (1339).

(14) Schulze, T. F.; Schmidt, T. W. Photochemical Upconversion: Present Status and Prospects for Its Application to Solar Energy Conversion. *Energy Environ. Sci.* **2015**, *8* (1), 103–275.

(15) Nattestad, A.; Cheng, Y. Y.; MacQueen, R. W.; Schulze, T. F.; Thompson, F. W.; Mozer, A. J.; Fückel, B.; Khoury, T.; Crossley, M. J.; Lips, K. Dye-Sensitized Solar Cell with Integrated Triplet–Triplet Annihilation Upconversion System. *J. Phys. Chem. Lett.* **2013**, *4* (12), 2073–2078.

(16) Castellano, F. N.; McCusker, C. E. MLCT Sensitizers in Photochemical Upconversion: Past, Present, and Potential Future Directions. *Dalton Trans.* **2015**, *44* (41), 17906–17910.

(17) Singh-Rachford, T. N.; Castellano, F. N. Low Power Visible-to-UV Upconversion. *J. Phys. Chem. A* **2009**, *113* (20), 5912–5917.

(18) Zhao, W.; Castellano, F. N. Upconverted Emission from Pyrene and Di-Tert-Butylpyrene Using Ir (Ppy) 3 as Triplet Sensitizer. *J. Phys. Chem. A* **2006**, *110* (40), 11440–11445.

(19) Sugunan, S. K.; Tripathy, U.; Brunet, S. M. K.; Paige, M. F.; Steer, R. P. Mechanisms of Low-Power Noncoherent Photon Upconversion in Metalloporphyrin−Organic Blue Emitter Systems in Solution. *J. Phys. Chem. A* **2009**, *113* (30), 8548–8556.

(20) Singh-Rachford, T. N.; Castellano, F. N. Triplet Sensitized Red-to-Blue Photon Upconversion. *J. Phys. Chem. Lett.* **2010**, *1* (1), 195–200.

(21) Islangulov, R. R.; Lott, J.; Weder, C.; Castellano, F. N. Noncoherent Low-Power Upconversion in Solid Polymer Films. *J. Am. Chem. Soc.* **2007**, *129* (42), 12652–12653.

(22) Monguzzi, A.; Tubino, R.; Meinardi, F. Multicomponent Polymeric Film for Red to Green Low Power Sensitized Up-Conversion. *J. Phys. Chem. A* **2009**, *113* (7), 1171–1174.

(23) Merkel, P. B.; Dinnocenzo, J. P. Low-Power Green-to-Blue and Blue-to-UV Upconversion in Rigid Polymer Films. *J. Lumin.* **2009**, *129* (3), 303–306.

(24) Atkins, P. W.; Friedman, R. S. *Molecular Quantum Mechanics*; Oxford University Press, USA, **2011**.

(25) Condon, E. U.; Shortley, G. H. *The Theory of Atomic Spectra*; Cambridge University Press, **1935**.

(26) Förster, T. Energy Migration and Fluorescence. *J. Biomed. Opt.* **2012**, *17* (1), 011002–011002.

(27) Deng, F.; Blumhoff, J.; Castellano, F. N. Annihilation Limit of a Visible-to-UV Photon Upconversion Composition Ascertained from Transient Absorption Kinetics. *J. Phys. Chem. A* **2013**, *117* (21), 4412–4419.

(28) Giachino, G. G.; Kearns, D. R. Nature of the External Heavy-atom Effect on Radiative and Nonradiative Singlet–Triplet Transitions. *J. Chem. Phys.* **1970**, *52* (6), 2964–2974.

(29) Murphy, C. B.; Zhang, Y.; Troxler, T.; Ferry, V.; Martin, J. J.; Jones, W. E. Probing Förster and Dexter Energy-Transfer Mechanisms in Fluorescent Conjugated Polymer Chemosensors. *J. Phys. Chem. B* **2004**, *108* (5), 1537–1543.

(30) Jang, S.; Shin, K. J.; Lee, S. Effects of Excitation Migration and Translational Diffusion in the Luminescence Quenching Dynamics. *J. Chem. Phys.* **1995**, *102* (2), 815–827.

(31) Sudha, K.; Sundharamurthi, S.; Karthikaikumar, S.; Abinaya, K.; Kalimuthu, P. Switching of Forster to Dexter Mechanism of Short-Range Energy Transfer in Meso-Anthrylporphyrin. *J. Phys. Chem. C* **2017**, *121* (11), 5941–5948.

(32) Ventura, B.; Barigelletti, F.; Lodato, F.; Officer, D. L.; Flamigni, L. Energy Transfer Processes in Electronically Coupled Porphyrin Hetero-Dyads Connected at the β Position. *Phys. Chem. Chem. Phys.* **2009**, *11* (13), 2166–2176.

(33) Nickel, B. Delayed Fluorescence from Upper Excited Singlet States Sn (N> 1) of the Aromatic Hydrocarbons 1, 2-benzanthracene, Fluoranthene, Pyrene, and Chrysene in Methylcyclohexane. *Helv. Chim. Acta* **1978**, *61* (1), 198–222.

(34) GeorgeáTruscott, T. Faraday Communications. Efficiency of Triplet-Photosensitised Singlet Oxygen Generation in Benzene. *J. Chem. Soc. Faraday Trans.* **1990**, *86* (14), 2671–2672.

(35) Bachilo, S. M.; Weisman, R. B. Determination of Triplet Quantum Yields from Triplet−Triplet Annihilation Fluorescence. *J. Phys. Chem. A* **2000**, *104* (33), 7711–7714.

(36) Levin, P. P.; Costa, S. M. B.; Nunes, T. G.; Vieira Ferreira, L. F.; Ilharco, L. M.; Botelho Do Rego, A. M. Kinetics of Triplet−Triplet Annihilation of Tetraphenylporphyrin in Liquid and Frozen Films of Decanol on the External Surface of Zeolite. Fast Probe Diffusion in Monolayers and Polycrystals. *J. Phys. Chem. A* **2003**, *107* (3), 328–336.

(37) Jankus, V.; Snedden, E. W.; Bright, D. W.; Whittle, V. L.; Williams, J. A. G.; Monkman, A. Energy Upconversion via Triplet Fusion in Super Yellow PPV Films Doped with Palladium Tetraphenyltetrabenzoporphyrin: A Comprehensive Investigation of Exciton Dynamics. *Adv. Funct. Mater.* **2013**, *23* (3), 384–393.

(38) Saltiel, J.; Atwater, B. W. Spin-Statistical Factors in Diffusion-Controlled Reactions. In *Advances in Photochemistry*; John Wiley & Sons, Ltd, 1988; pp 1–90.

(39) Cheng, Y. Y.; Khoury, T.; Clady, R. G. C. R.; Tayebjee, M. J. Y.; Ekins-Daukes, N. J.; Crossley, M. J.; Schmidt, T. W. On the Efficiency Limit of Triplet–Triplet Annihilation for Photochemical Upconversion. *Phys Chem Chem Phys* **2010**, *12* (1), 66–71.

(40) Cheng, Y. Y.; Fückel, B.; Khoury, T.; Clady, R. G. C. R.; Tayebjee, M. J. Y.; Ekins-Daukes, N. J.; Crossley, M. J.; Schmidt, T. W. Kinetic Analysis of Photochemical Upconversion by Triplet−Triplet Annihilation: Beyond Any Spin Statistical Limit. *J. Phys. Chem. Lett.* **2010**, *1* (12), 1795–1799.

(41) Parker, C. A.; Bowen, E. J. Sensitized P-Type Delayed Fluorescence. *Proc. R. Soc. Lond. Ser. Math. Phys. Sci.* **1997**, *276* (1364), 125–135.

(42) Manna, M. K.; Shokri, S.; Wiederrecht, G. P.; Gosztola, D. J.; Ayitou, A. J.-L. New Perspectives for Triplet–Triplet Annihilation Based Photon Upconversion Using All-Organic Energy Donor & Acceptor Chromophores. *Chem. Commun.* **2018**, *54* (46), 5809–5818.

(43) *Delayed Fluorescence and Some Properties of the Chlorophyll Triplets - Parker - **1967** - Photochemistry and Photobiology - Wiley Online Library*.

(44) Parker, C. A.; Hatchard, C. G. Triplet-Singlet Emission in Fluid Solutions. Phosphorescence of Eosin. *Trans. Faraday Soc.* **1961**, *57*, 1894.

(45) Schmidt, T. W.; Castellano, F. N. Photochemical Upconversion: The Primacy of Kinetics. *J. Phys. Chem. Lett.* **2014**, *5* (22), 4062–4072.

(46) Awwad, N. *Merging of Triplet Fusion Processes Sensitized by Metalloporphyrins with Photopolymerization Applications*; North Carolina State University, 2020.

(47) Monguzzi, A.; Tubino, R.; Meinardi, F. Upconversion-Induced Delayed Fluorescence in Multicomponent Organic Systems: Role of Dexter Energy Transfer. *Phys. Rev. B* **2008**, *77* (15), 155122.

(48) Haefele, A.; Blumhoff, J.; Khnayzer, R. S.; Castellano, F. N. Getting to the (Square) Root of the Problem: How to Make Noncoherent Pumped Upconversion Linear. *J. Phys. Chem. Lett.* **2012**, *3* (3), 299–303.

(49) Auckett, J. E.; Chen, Y. Y.; Khoury, T.; Clady, R. G. C. R.; Ekins-Daukes, N. J.; Crossley, M. J.; Schmidt, T. W. Efficient Up-Conversion by Triplet-Triplet Annihilation. *J. Phys. Conf. Ser.* **2009**, *185* (1), 012002.

(50) McCusker, C. E.; Castellano, F. N. Efficient Visible to Near-UV Photochemical Upconversion Sensitized by a Long Lifetime Cu(I) MLCT Complex. *Inorg. Chem.* **2015**, *54* (12), 6035–6042.

(51) Zhou, Y.; Castellano, F. N.; Schmidt, T. W.; Hanson, K. On the Quantum Yield of Photon Upconversion via Triplet–Triplet Annihilation. *ACS Energy Lett.* **2020**, *5* (7), 2322–2326.

(52) Demchenko, A. P.; Tomin, V. I.; Chou, P.-T. Breaking the Kasha Rule for More Efficient Photochemistry. *Chem. Rev.* **2017**, *117* (21), 13353–13381.

(53) Karolczak, J.; Kowalska, D.; Lukaszewicz, A.; Maciejewski, A.; Steer, R. P. Photophysical Studies of Porphyrins and Metalloporphyrins: Accurate Measurements of Fluorescence Spectra and Fluorescence Quantum Yields for Soret Band Excitation of Zinc Tetraphenylporphyrin. *J. Phys. Chem. A* **2004**, *108* (21), 4570–4575.

(54) Stelmakh, G. F; Tsvirko, M. P. Delayed Fluorescence from the Upper Excited Electronic States of Metalloporphyrins. *Opt. Spectrosc.* **1980**, *49* (3), 278–281.

(55) Skoog, D. A.; Holler, F. J.; Crouch, S. R. *Principles of Instrumental Analysis*, 6th ed.; Cengage Learning: Boston, MA, **2018**.

(56) *Handbook of Spectroscopy*, 1st ed.; Gauglitz, G.; Vo-Dinh, T.; Eds.; Wiley, **2003**.

(57) Czerny, M.; Turner, A. F. Astigmatismus Bei Spiegelspektrometern. *Z. Für Phys.* **1930**, *61* (11), 792–797.

(58) Shafer, A. B.; Megill, L. R.; Droppleman, L. Optimization of the Czerny–Turner Spectrometer. *J. Opt. Soc. Am.* **1964**, *54* (7), 879–887.

(59) Swinehart, D. F. The Beer-Lambert Law. *J. Chem. Educ.* **1962**, *39* (7), 333–335.

(60) Beer. Bestimmung Der Absorption Des Rothen Lichts in Farbigen Flüssigkeiten. *Ann. Phys. Chem.* **1852**, *162* (5), 78–88.

(61) Balzani, V.; Ceroni, P.; Juris, A. *Photochemistry and Photophysics*; Wiley-VCH Verlag GmbH & Co. KGaA, **2014**.

(62) Lakowicz, J. R. *Principles of Fluorescence Spectroscopy*, 3rd ed.; Springer: Boston, MA, 2006.

(63) Berera, R.; van Grondelle, R.; Kennis, J. T. M. Ultrafast Transient Absorption Spectroscopy: Principles and Application to Photosynthetic Systems. *Photosynth. Res.* **2009**, *101* (2), 105–118.

(64) Rosko, M. C. *Photophysical Investigation of Cuprous bisphenanthroline Chromophores*; North Carolina State University, **2024**.

(65) Wigner, E. Nschr. Akad. Wiss. Goettingen. Math Physik, KI, IIa, **1927**, 375.

Chapter 2: Homomolecular Triplet-Triplet Annihilation in Metalloporphyrin Photosensitizers

The contents of this chapter have been published in the *Journal of Physical Chemistry A*.

Arshad, A.; Castellano, F. N. Homomolecular Triplet–Triplet Annihilation in Metalloporphyrin Photosensitizers. *J. Phys. Chem. A* **2024**, *128*, 7648-7656.

https://doi.org/10.1021/acs.jpca.4c05052

Introduction

Photochemical upconversion, resulting from sensitized triplet fusion or triplet-triplet annihilation (TTA), is a well-established mechanism leveraging two sequential triplet-triplet energy transfer (TTET) processes between photosensitizer and acceptor molecules.[1–10] These consecutive energy transfer events convert two low-frequency photons into one high-energy photon or one higher-lying singlet excited state. TTA is governed by bimolecular reaction kinetics between two excited molecules. It is therefore a diffusion-controlled process in solution, requiring two molecules in their triplet excited states to be within the molecular orbital overlap limits of Dexter-type energy transfer processes.[1–10] High-yielding TTA processes mandate a large population of excited triplets, so virtually all factors directly or indirectly affecting this energized population are paramount.

The photosensitizer molecule should not only have strong absorbance (high molar extinction coefficients) in the visible to near infra-red regions of the electromagnetic spectrum – so that many excited singlets can be formed – but also have a high ISC rate – so that there is efficient and ideally quantitative conversion to the triplet excited state of the photosensitizer. In cases where the molecule does not have a high molar extinction coefficient, high photosensitizer concentrations are required to circumvent this limitation.[11–21] To ensure high ISC rates, heavy metal ions like

palladium and platinum – owing to their large spin-orbit coupling constants – are incorporated into the photosensitizer, ensuring near unity ISC yields.[22–29] Since bimolecular TTET is diffusion-controlled in solution, efficient energy transfer between the excited triplets of the photosensitizer and acceptor chromophore requires the photosensitizer to have a long-lived excited triplet state poised for exothermic TTET with the acceptor. Moreover, molecular oxygen (a ground state triplet) can not only supplement back ISC to the ground state of the photosensitizer molecules,[30,31] it can also engage in Dexter energy transfer with any excited triplet populations having an energy equal to or greater than 0.98 eV, producing singlet excited O_2, $^1\Delta_g$.[32] Therefore, molecular oxygen will significantly diminish triplet populations while producing highly reactive and long-lived singlet oxygen species capable of forming endoperoxides with popular acceptor chromophores.[33] Lastly, the acceptor molecules should have a high fluorescence quantum yield, and the energy of two excited triplet acceptor molecules should be greater than or equal to the excited singlet for the triplet fusion to be feasible.[34–38]

Metalloporphyrin photosensitizers have established themselves as excellent triplet photosensitizers for sensitized TTA upconversion processes based on the abovementioned properties.[13,39–48] These metal-centered porphyrin derivatives exhibit characteristic properties like strong absorption in the visible region of the electromagnetic spectrum, long-lived excited state triplets, and efficient ISC (particularly in the ones containing heavy metals).[49] Although Parker and Hatchard reported TTA in solution in the early 1960s,[50] the research was limited to using all organic chromophores as photosensitizers and acceptors for the rest of the 20th century. The true potential of this light-harvesting/wavelength-shifting technology was realized in the early 2000s when Castellano et al.[51,52] and Baluschev et al.[53–55] successfully demonstrated the use of transition metal complexes as photosensitizers for heteromolecular TTA. Subsequently, sensitized TTA

reactions have realized applications in numerous fields, including photovoltaics,[56] biosensing,[57] cancer therapeutics,[58–60] photoredox catalysis,[61–63] and photopolymerization.[4,64–66]

Scheme 0.1 Qualitative Jablonski Diagram Illustrating (a) Heteromolecular Sensitized TTA-Based Upconversion; (b) Homomolecular TTA-Based Upconversion Leading to Population of the S_2 Excited State in Metalloporphyrins.[a]

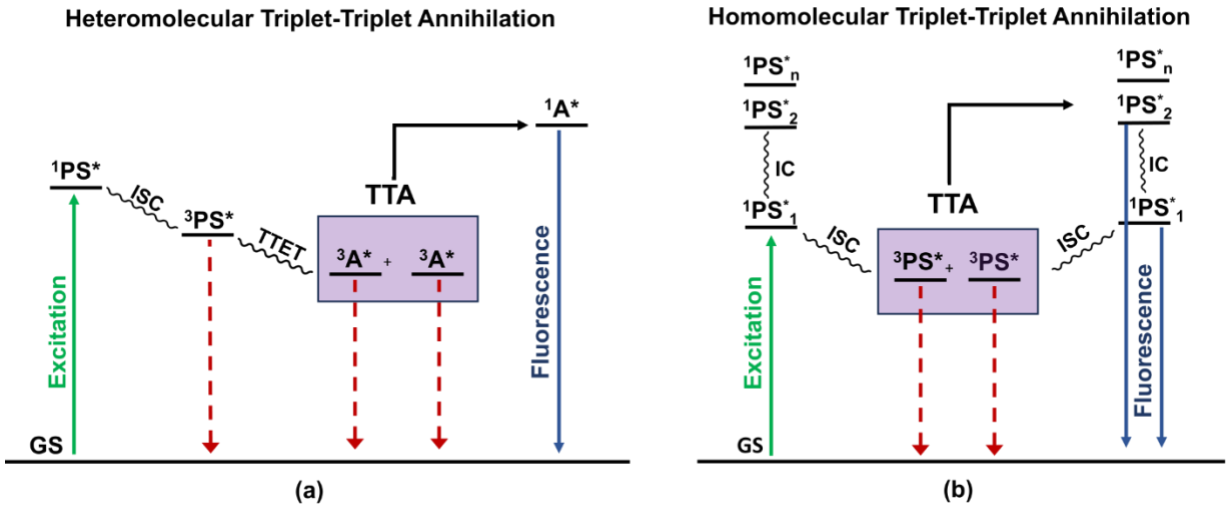

aGS = Ground State, PS = Photosensitizer, ISC = Intersystem Crossing, TTET = Triplet-Triplet Energy Transfer, A = Acceptor/Annihilator, TTA = Triplet-Triplet Annihilation, IC = Internal Conversion.

The traditional heteromolecular mechanism of TTA utilizes two different molecules for the roles of a photosensitizer and an acceptor. In *homomolecular* triplet-triplet annihilation (HTTA), two identical molecules act as the photosensitizer and the acceptor. Scheme 2.1 presents the mechanism for this process, highlighting the main differences between the hetero- and homomolecular TTA. In heteromolecular TTA systems, the emission is observed from the lowest excited singlet state of the acceptor, whereas in homomolecular TTA systems, the excited singlet state (^1PS_n* where n > 1) responsible for light emission or production of the requisite dark state is higher than the one formed upon excitation ($^1PS_1$*). This phenomenon violates Kasha's rule, which states that only the lowest excited state of a given multiplicity accounts for observable light emission.[67] Since the

emission is observed from a forbidden transition from the upper excited states with low quantum yield ($<10^{-3}$) and short lifetime (typically several picoseconds), it becomes crucial to use a high-power excitation source along with a sensitive detection system.[68] Consequently, HTTA is underexplored due to the unique challenges accompanying its study relative to the traditional heteromolecular TTA. Systems based on aromatic thiones, non-alternant aromatic hydrocarbons, and metalloporphyrins are some of the few examples demonstrating HTTA.[68–70] Tsvirko and Stelmakh pioneered observations of delayed S_2 fluorescence resulting from homomolecular TTA in metalloporphyrins.[70,71] Delayed S_2 fluorescence has also been identified in molecular families with optimal electronic energy gaps and triplet lifetimes.[72] Recently, our group utilized the potential energy stored in this homomolecular TTA process in the S_2 excited state for achieving green and yellow visible light activation of free radical polymerization in a triacrylate monomer using zinc(II) tetraphenylporphyrin (ZnTPP),[64] which led to applications in 3D printing of plastics.[65,66,73]

The current investigation employs transient absorption spectroscopy to investigate bimolecular HTTA processes in widely employed metalloporphyrin photosensitizers. The photosensitizers used in this study include ZnTPP, palladium(II) octaethylporphyrin (PdOEP), platinum(II) octaethylporphyrin (PtOEP), and platinum(II) tetraphenyltetrabenzoporphyrin (PtTPBP). We also used nickel(II) tetraphenylporphyrin (NiTPP) as a control sample in this study as it is known to be rapidly quenched intramolecularly through ligand-field state deactivation[74–76] and, therefore, cannot engage in HTTA chemistry.

Transient absorption spectroscopy (laser flash photolysis) is a powerful pump-probe spectroscopic technique that provides detailed insights into excited state species' electronic and structural dynamics on chemically relevant time scales. Ultrafast transient absorption spectroscopy is also

valuable, offering high temporal resolution on the femtosecond and nanosecond time scales, allowing the interrogation and quantification of nonemissive or "dark" excited states that cannot be quantified by the traditional fluorescence spectroscopy associated with upconversion processes. In this study, we aim to establish the significance of HTTA, which proves to be a competitive process to heteromolecular TTA in which these common metalloporphyrins are employed. These findings add to the fundamental understanding of excited state dynamics in metalloporphyrins and have implications for optimizing their performance in both homo- and heteromolecular TTA-based photochemistry. In the pursuit of this project, triplet excited state extinction coefficients were determined in all of these metalloporphyrins, three of them for the first time, using ultrafast transient absorption spectroscopy in conjunction with singlet depletion.

Methods

Reagents and Chemicals

ZnTPP and NiTPP were procured from Sigma-Aldrich and used without further purification. PtOEP, PtTPBP, and PdOEP were obtained from Frontier scientific and used as received. Spectroscopic grade toluene, sourced from Sigma-Aldrich, was utilized as received.

Sample Preparation for Photophysical Measurements

The absorption and emission samples were prepared in standard 1 cm^2 quartz cuvettes. Samples with a concentration of 0.05 mM were used to obtain the room-temperature emission spectra. Before all light emission measurements, the samples were degassed with a stream of argon and then photoexcited at 380 nm. Samples intended for nanosecond transient absorption measurements had ground state absorptions ranging from 0.3 to 0.6 optical density at the excitation wavelength. They underwent at least three freeze-pump-thaw degas cycles in a specially designed 1 cm^2 optical

cell attached to a side-arm round-bottomed flask. All solutions used in the photophysical measurements were prepared using spectroscopic grade toluene.

Photophysical Measurements

A Cary 60 Bio UV-vis spectrophotometer from Agilent Technologies was utilized for steady-state absorption spectra, while emission spectra were recorded using a Cary Eclipse Fluorimeter, also from Agilent Technologies. Nanosecond transient absorption measurements were conducted using an LP920 spectrometer (Edinburgh Instruments) equipped with an Andor iStar iCCD detector. Excitation was achieved with a Nd:YAG/OPO laser system (Opotek Radiant QX4130) operating at 1 Hz. In all kinetic and spectral absorption measurements, samples demonstrated a linear relationship between ΔA and pulse energy at the detection wavelength (Figure S2.10). Power-dependence experiments involved adjusting the incident laser pulse energy with neutral density filters, and pulse energies were measured using a Coherent Fieldmate power meter. Single wavelength absorption kinetics were analyzed using Origin 2023b software. Please refer to the Supporting Information for the femtosecond transient absorption spectroscopy used to determine the triplet extinction coefficients through singlet depletion.[77]

Results and Discussion

The molecular structures of the metalloporphyrins employed in this study are collected in Figure 2.1. The normalized absorption and total emission spectra of these metalloporphyrins are presented in Figure 2.2. The absorption spectra of the porphyrin systems are characterized by two strong absorption bands known as the Soret and Q bands that involve ligand-centered $\pi-\pi^*$ transitions. The Q bands are typically in the 500-650 nm region. The lower energy peak in the Q band corresponds to the electronic origin Q (0,0) of the transition in the first excited singlet state

(S_1). In contrast, the higher energy peak corresponds to a vibrational overtone Q (1,0). The highly intense Soret, the B band in the 380-430 nm region, forms the second characteristic feature in the absorption spectrum of the porphyrins. It represents the transition into the electronic origin B (0,0) of the second excited singlet state (S_2). The emission features mirror the absorption features in the respective Q-bands.[78]

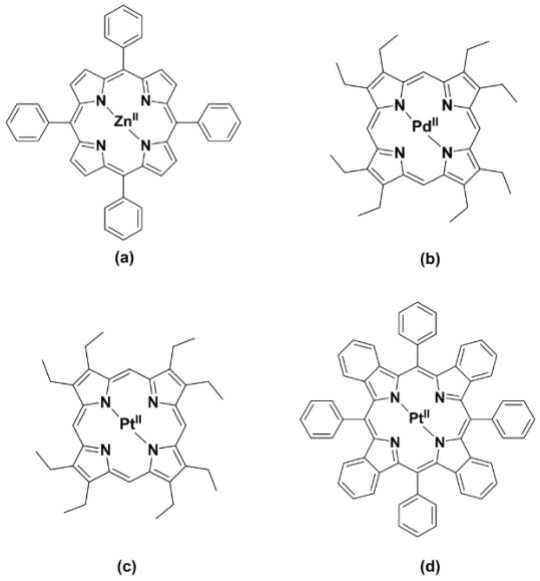

Figure 0.1 Chemical structures of (a) ZnTPP, (b) PdOEP, (c) PtOEP, and (d) PtTPBP.

As mentioned earlier, ZnTPP (Figure 2.1a) is one of the few compounds that display a measurable S_2 emission at RT, unlike the other porphyrins investigated here.[79–81] The higher energy excited states non-radiatively relax to the first excited singlet state on picosecond time scales, hence enabling the observation of fluorescence from S_1 and phosphorescence from T_1 at room temperature in PdOEP, PtOEP, and PtTPBP due to spin-orbit coupling.[82,83]

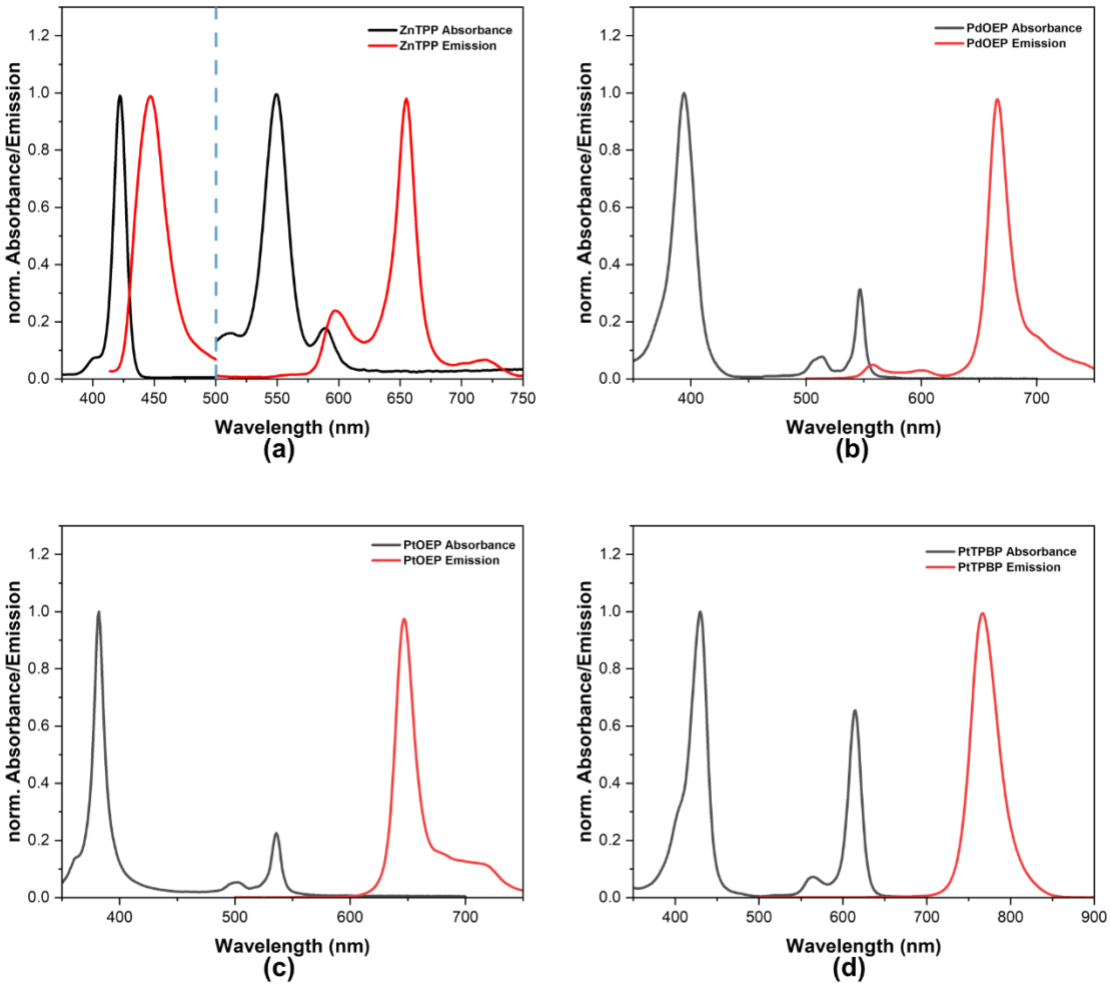

Figure 0.2 Normalized absorption (black) and total emission (red) spectra for metalloporphyrins measured in degassed toluene at room temperature (a) ZnTPP, (b) PdOEP, (c) PtOEP, and (d) PtTPBP.

The excited state triplets in metalloporphyrin photosensitizers are proposed to decay through parallel first- and second-order pathways, as described in eq 2.1.

$$\frac{d[^3PS^*]_t}{dt} = -k_T[^3PS^*]_t - k_{TT}[^3PS^*]_t^2 \qquad \textbf{eq 2.1}$$

The first-order decay rate constant (k_T) encompasses all intramolecular triplet decay processes and any pseudo-first-order quenching by dissolved molecular oxygen.[84] In contrast, the second-order

decay rate constant (k_{TT}) accounts explicitly for TTA between two triplet-excited metalloporphyrin molecules. Eq 2.1 has been solved analytically, yielding eq 2.2.[12,19,85]

$$\frac{[^3PS^*]_t}{[^3PS^*]_o} = \frac{1-\beta}{e^{k_T t}-\beta}\,;\ \beta = \frac{\alpha}{k_T+\alpha} \text{ and } \alpha = k_{TT}[^3PS^*]_o \qquad \textbf{eq 2.2}$$

Here, $[^3PS^*]_t$ denotes the time-varying concentration of sensitized triplets, $[^3PS^*]_0$ is the initial concentration of excited triplets, k_T is the first-order triplet decay rate constant, k_{TT} is the second-order TTA rate constant, and β represents the fraction of sensitized triplets decaying via TTA. Eq 2.2 is further reformulated as eq 2.3 to incorporate relevant transient absorption parameters, as the concentration of excited triplets directly correlates with ΔA.[86]

$$\Delta A_t = \frac{\Delta A_o(1-\beta)}{e^{k_T t}-\beta} \qquad \textbf{eq 2.3}$$

These mathematical expressions simplify the complex kinetics governing triplet decay and TTA processes in metalloporphyrin systems, providing a quantitative framework for understanding their photophysical behavior. We recorded transient absorption measurements for all samples and analyzed the data using eq 2.3 with nonlinear least-squares fitting in Origin 2023b. This approach allowed us to extract three crucial parameters: ΔA_0, β, and k_T. Figure 2.3 illustrates a representative curve fitting of transient absorption decay for ZnTPP using eq 2.3. The figure highlights excellent agreement between fitted values and the kinetic model across measurements conducted under varying laser pulse energies (the remaining kinetic fits are provided in the Supporting Information). Due to rapid deactivation through ligand-field states,[74–76] NiTPP exhibited no triplet signature in the nanosecond transient absorption difference spectrum, Figure S2.11. NiTPP, therefore, cannot exhibit any TTA processes due to their picosecond triplet lifetimes and represents a useful negative control sample in comparative studies.

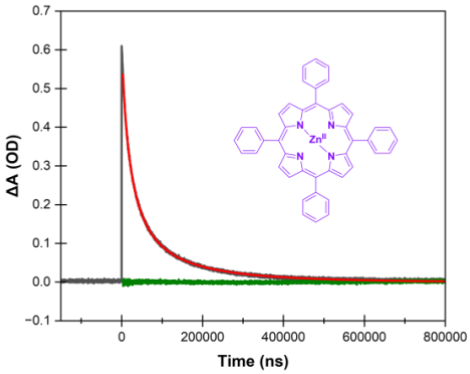

Figure 0.3 Representative transient absorption kinetic decay (black) of triplet ZnTPP at 470 nm produced using 514 nm excitation (7.1 mJ, 5-7 ns fwhm) in 0.05 mM of ZnTPP in freeze-pump-thaw degassed toluene. The red line represents the kinetic fit of the experimental data to eq 2.3, and the green line shows the residuals of the fit.

To determine the initial concentration of excited triplets, $[^3PS^*]_0$, each sample's triplet extinction coefficient (ε_t) needed to be determined. While the ε_t value for triplet ZnTPP (71,000 $M^{-1}cm^{-1}$) was available from the literature[87], the corresponding values for triplet PdOEP, PtOEP, and PtTPBP have not been previously reported. We experimentally determined these values for all of the metalloporphyrins in this study using femtosecond transient absorption spectroscopy in combination with singlet depletion: ZnTPP ($\varepsilon_{t\,(470\ nm)}$ = 78,000 $M^{-1}cm^{-1}$), PdOEP $\varepsilon_{t\,(430\ nm)}$ = 67,000 $M^{-1}cm^{-1}$), PtOEP ($\varepsilon_{t\,(418\ nm)}$ = 51,000 $M^{-1}cm^{-1}$), and PtTPBP ($\varepsilon_{t\,(460\ nm)}$ = 100,000 $M^{-1}cm^{-1}$), see Supporting Information. Using β and k_T as derived fitting parameters, we calculated α and the second-order TTA rate constant (k_{TT}). Detailed results from these kinetic analyses are presented in Tables 2.1 (ZnTPP), 2.2 (PdOEP), 2.3 (PtOEP), and 2.4 (PtTPBP).

Table 0.1 Kinetic Parameters Obtained From the Fits of Transient Absorption Decay of ZnTPP at 470 nm to eq 2.3.[b]

$\varepsilon_{t\,(470\,nm)}$ (10^4 $M^{-1}cm^{-1}$)	Pulse energy (mJ)	k_T (10^3 s^{-1})	$[^3PS^*]_o$ (10^{-6} M)	β	α (10^4 s^{-1})	k_{TT} (10^9 $M^{-1}s^{-1}$)
7.8	2.2	3.4	3.21	0.859	2.08	6.5
	3.7	3.5	4.87	0.889	2.80	5.8
	5.8	4.3	6.67	0.894	3.58	5.4
	7.1	4.3	7.82	0.904	4.06	5.2
	8.4	4.9	9.74	0.899	4.39	4.5

[b]See text for the descriptions for the kinetic fit parameters.

Table 0.2 Kinetic Parameters Obtained From the Fits of Transient Absorption Decay of PdOEP at 430 nm to eq 2.3.[c]

$\varepsilon_{t\,(430\,nm)}$ (10^4 $M^{-1}cm^{-1}$)	Pulse energy (mJ)	k_T (10^3 s^{-1})	$[^3PS^*]_o$ (10^{-6} M)	β	α (10^4 s^{-1})	k_{TT} (10^{10} $M^{-1}s^{-1}$)
6.7	2.1	3.9	0.55	0.627	0.65	1.2
	2.6	4.1	0.68	0.633	0.71	1.0
	3.3	3.5	0.85	0.729	0.96	1.1
	4.1	3.8	1.06	0.733	1.05	0.99
	5.2	2.9	1.38	0.839	1.51	1.1

[c]See text for the descriptions for the kinetic fit parameters.

Table 0.3 Kinetic Parameters Obtained From the Fits of Transient Absorption Decay of PtOEP at 418 nm to eq 2.3.[d]

$\varepsilon_{t\,(418\,nm)}$ (10^4 $M^{-1}cm^{-1}$)	Pulse energy (mJ)	k_T (10^4 s^{-1})	$[^3PS^*]_o$ (10^{-6} M)	β	α (10^4 s^{-1})	k_{TT} (10^9 $M^{-1}s^{-1}$)
5.1	3.7	1.2	4.94	0.745	3.64	7.4
	4.1	1.4	5.37	0.717	3.56	6.6
	4.7	1.2	6.08	0.782	4.38	7.2
	5.4	1.1	6.97	0.818	5.02	7.2
	5.8	1.2	7.68	0.815	5.28	6.9

[d]See text for the descriptions for the kinetic fit parameters.

Table 0.4 Kinetic parameters obtained from the fits of transient absorption decay of PtTPBP at 460 nm to eq 2.3.[e]

$\varepsilon_{t\,(460\,nm)}$ (10^4 $M^{-1}cm^{-1}$)	Pulse energy (mJ)	k_T (10^4 s^{-1})	$[^3PS^*]_o$ (10^{-6} M)	β	α (10^4 s^{-1})	k_{TT} (10^{10} $M^{-1}s^{-1}$)
10	2.6	2.2	0.80	0.351	1.21	1.5
	3.2	2.1	0.95	0.454	1.72	1.8
	3.9	2.1	1.11	0.456	1.78	1.6
	5.2	2.2	1.48	0.502	2.19	1.5
	6.6	2.1	1.70	0.544	2.54	1.5

[e]See text for the descriptions for the kinetic fit parameters.

As apparent from visual inspection of the data collected in Tables 1-4, increasing the laser pulse excitation energy increases the excited state triplet population of the photosensitizer. This, in turn, means that more excited state triplets are available to engage in the TTA event, thus facilitating

the HTTA process, reflected in the increasing β values. The average values of the first order rate constants (k_T) for this series lie in the range of 10^3-10^4 s^{-1}, with the slowest value at 3.6 x 10^3 s^{-1} in PdOEP to the fastest value of 2.1 x 10^4 s^{-1} in PtTPBP. The k_T values for ZnTPP (4.0 x 10^3 s^{-1}) and PtOEP (1.2 x 10^4 s^{-1}) are sandwiched between PdOEP and PtTPBP. As previously mentioned, this k_T value includes the first-order decay and pseudo-first-order quenching processes; the latter is dominated by dissolved molecular oxygen in the sample solution. Thus, better deoxygenation of the sample solutions will translate into a longer-lived triplet excited state and slower first-order decay constant.

The lack of scatter in the k_T values, when incident pulse energy is varied across these metalloporphyrins, is due to the experimental limitation of the sample deoxygenation. Platinum is the heaviest metal center in this series and, thus, has the highest spin-orbit coupling constant, leading to a higher efficiency of ISC from the singlet to the triplet excited state as well as a higher efficiency of the triplet-energy transfer to dissolved molecular oxygen. These properties rationalize why the Pt(II) complexes feature larger k_T values when all the solutions were subjected to identical deoxygenation conditions: the platinum triplet excited states have more time to interact with the remnants of molecular oxygen and engage in quenching processes compared to the other two samples.

Notably, the somewhat random scatter in the k_T values also suggests that self-quenching dynamics do not play a role here. If self-quenching were efficient, the k_T values would have significantly increased with the increasing triplet concentration (increasing incident pulse energies) which is not the case in this investigation. Self-quenching between two excited triplets could also occur via photoinduced electron transfer, yielding the one-electron oxidized and one-electron reduced species of the sensitizer, termed ionogenesis.[88] The transient absorption traces decay back to

baseline on time scales much shorter than that required for electron-hole recombination (milliseconds), which implies that long-lived radicals are not produced. Additionally, no spectroscopic evidence exists for forming radical cations or anions in any of the molecules under investigation. We, therefore, posit that long-lived radical species do not represent a significant decay pathway in these systems. The HTTA rate constants (k_{TT}) lie in the range of 10^9-10^{10} $M^{-1}s^{-1}$, correlating to diffusion- or near-diffusion-controlled reactions. The slowest rate second-order constant for HTTA is exhibited by ZnTPP with a k_{TT} value of 5.5 x 10^9 $M^{-1}s^{-1}$, and the fastest rate constant is reflected in the k_{TT} value of PtTPBP at 1.6 x 10^{10} $M^{-1}s^{-1}$. The rates of HTTA in PtOEP and PdOEP lie in between with k_{TT} values of 7.1 x 10^9 $M^{-1}s^{-1}$ in PtOEP and 1.1 x 10^{10} $M^{-1}s^{-1}$ in PdOEP.

This quantification of triplet extinction coefficients and rate constants governing the bimolecular triplet decay in the metalloporphyrins under study here has provided valuable insights that can be leveraged to optimize the performance of photon upconversion in various energy harvesting applications. The HTTA process offers several advantages over traditional sensitized TTA. Firstly, HTTA is a single-component system where the formulation relies solely on the photosensitizer. This eliminates energy transfer steps between the photosensitizer and a separate annihilator, simplifying the system and reducing potential interference from competing reactions or byproducts. Furthermore, the ultrafast nature of the upper excited states involved in HTTA (on the picosecond time scale) enables driving rapid photochemical transformations, such as polymerizations, that can take advantage of this high-energy process. While there are challenges associated with this approach, the inherent benefits of a simplified, single-component system make HTTA a promising strategy for various photochemical applications.

Conclusions

In this study, we have successfully conducted a quantitative investigation into HTTA using established metalloporphyrin photosensitizers. Employing femto- and nanosecond transient absorption spectroscopy, we determined the excited state triplet extinction coefficients in all of these molecules and rigorously analyzed transient absorption kinetics to determine the first- and second-order rate constants (k_T and k_{TT}) governing the HTTA phenomenon in these sensitizers. By elucidating the dynamics of excited state interactions between these photosensitizers, this study advances fundamental scientific knowledge and lays the groundwork for executing kinetic analyses of pathways competitive with heteromolecular TTA that use metalloporphyrins. Such knowledge will impact future innovations in diverse fields, including photochemical upconversion, free radical polymerization, photoredox catalysis, 3D printing, and photochemistry driven from upper excited states in molecules and materials.

Acknowledgment

This work was funded through BioLEC, an Energy Frontier Research Center of the U.S. Department of Energy, Office of Science, Office of Basic Energy Sciences, under Award DE-SC0019370.

Supporting Information Available

Additional static and transient absorbance spectra, static photoluminescence spectra, femtosecond transient absorption difference spectra, the calculations for determining the triplet extinction coefficient and triplet decay kinetics, and their associated fits to eq 2.3. See Section 2.8.

References

(1) Singh-Rachford, T. N.; Castellano, F. N. Photon Upconversion Based on Sensitized Triplet–Triplet Annihilation. *Coord. Chem. Rev.* **2010**, *254* (21), 2560–2573.

(2) Zhou, Y.; Castellano, F. N.; Schmidt, T. W.; Hanson, K. On the Quantum Yield of Photon Upconversion via Triplet–Triplet Annihilation. *ACS Energy Lett.* **2020**, *5* (7), 2322–2326.

(3) Feng, J.; Alves, J.; Clercq, D. M. de Schmidt, T. W. Photochemical Upconversion. *Annu. Rev. Phys. Chem.* **2023**, *74*, 145–168.

(4) Huang, L.; Han, G. Triplet–Triplet Annihilation Photon Upconversion-Mediated Photochemical Reactions. *Nat. Rev. Chem.* **2024**, *8* (4), 238–255.

(5) Richards, B. S.; Hudry, D.; Busko, D.; Turshatov, A.; Howard, I. A. Photon Upconversion for Photovoltaics and Photocatalysis: A Critical Review. *Chem. Rev.* **2021**, *121* (15), 9165–9195.

(6) Jin, J.; Yu, T.; Chen, J.; Hu, R.; Yang, G.; Zeng, Y.; Li, Y. Recent Advances of Triplet–Triplet Annihilation Upconversion in Photochemical Transformations. *Curr. Opin. Green Sustainable Chem.* **2023**, *43*, 100841.

(7) Ronchi, A.; Monguzzi, A. Sensitized Triplet–Triplet Annihilation Based Photon Upconversion in Full Organic and Hybrid Multicomponent Systems. *Chem. Phys. Rev.* **2022**, *3* (4), 041301.

(8) Castellano, F. N.; McCusker, C. E. MLCT Sensitizers in Photochemical Upconversion: Past, Present, and Potential Future Directions. *Dalton Trans.* **2015**, *44* (41), 17906–17910.

(9) Schulze, T. F.; Schmidt, T. W. Photochemical Upconversion: Present Status and Prospects for Its Application to Solar Energy Conversion. *Energy Environ. Sci.* **2015**, *8* (1), 103–125.

(10) Schmidt, T. W.; Castellano, F. N. Photochemical Upconversion: The Primacy of Kinetics. *J. Phys. Chem. Lett.* **2014**, *5* (22), 4062–4072.

(11) Kim, J.-H.; Deng, F.; Castellano, F. N.; Kim, J.-H. High Efficiency Low-Power Upconverting Soft Materials. *Chem. Mater.* **2012**, *24* (12), 2250–2252.

(12) Haefele, A.; Blumhoff, J.; Khnayzer, R. S.; Castellano, F. N. Getting to the (Square) Root of the Problem: How to Make Noncoherent Pumped Upconversion Linear. *J. Phys. Chem. Lett.* **2012**, *3* (3), 299–303.

(13) Monguzzi, A.; Borisov, S. M.; Pedrini, J.; Klimant, I.; Salvalaggio, M.; Biagini, P.; Melchiorre, F.; Lelii, C.; Meinardi, F. Efficient Broadband Triplet–Triplet Annihilation-Assisted Photon Upconversion at Subsolar Irradiance in Fully Organic Systems. *Adv. Funct. Mater.* **2015**, *25* (35), 5617–5624.

(14) Monguzzi, A.; Braga, D.; Gandini, M.; Holmberg, V. C.; Kim, D. K.; Sahu, A.; Norris, D. J.; Meinardi, F. Broadband Up-Conversion at Subsolar Irradiance: Triplet–Triplet Annihilation Boosted by Fluorescent Semiconductor Nanocrystals. *Nano Lett.* **2014**, *14* (11), 6644–6650.

(15) Hoseinkhani, S.; Tubino, R.; Meinardi, F.; Monguzzi, A. Achieving the Photon Up-Conversion Thermodynamic Yield Upper Limit by Sensitized Triplet–Triplet Annihilation. *Phys. Chem. Chem. Phys.* **2015**, *17* (6), 4020–4024.

(16) Monguzzi, A.; Mezyk, J.; Scotognella, F.; Tubino, R.; Meinardi, F. Upconversion-Induced Fluorescence in Multicomponent Systems: Steady-State Excitation Power Threshold. *Phys. Rev. B* **2008**, *78* (19), 195112.

(17) Cheng, Y. Y.; Khoury, T.; Clady, R. G. C. R.; Tayebjee, M. J. Y.; Ekins-Daukes, N. J.; Crossley, M. J.; Schmidt, T. W. On the Efficiency Limit of Triplet–Triplet Annihilation for Photochemical Upconversion. *Phys Chem Chem Phys* **2010**, *12* (1), 66–71.

(18) Mayr, C.; Schmidt, T. D.; Brütting, W. High-Efficiency Fluorescent Organic Light-Emitting Diodes Enabled by Triplet-Triplet Annihilation and Horizontal Emitter Orientation. *Appl. Phys. Lett.* **2014**, *105* (18), 183304.

(19) Cheng, Y. Y.; Fückel, B.; Khoury, T.; Clady, R. G. C. R.; Tayebjee, M. J. Y.; Ekins-Daukes, N. J.; Crossley, M. J.; Schmidt, T. W. Kinetic Analysis of Photochemical Upconversion by Triplet−Triplet Annihilation: Beyond Any Spin Statistical Limit. *J. Phys. Chem. Lett.* **2010**, *1* (12), 1795–1799.

(20) Schmidt, T. D.; Setz, D. S.; Flämmich, M.; Frischeisen, J.; Michaelis, D.; Mayr, C.; Rausch, A. F.; Wehlus, T.; Scholz, B. J.; Reusch, A. F.; et al. Comprehensive Efficiency Analysis of Organic Light-Emitting Diodes Featuring Emitter Orientation and Triplet-to-Singlet up-Conversion. *Appl. Phys. Lett.* **2013**, *103* (9), 093303.

(21) Singh-Rachford, T. N.; Castellano, F. N. Triplet Sensitized Red-to-Blue Photon Upconversion. *J. Phys. Chem. Lett.* **2010**, *1* (1), 195–200.

(22) Crites Tears, D. K.; McMillin, D. R. Exciplex Quenching of Photoexcited Platinum(II) Terpyridines: Influence of the Orbital Parentage. *Coord. Chem. Rev.* **2001**, *211* (1), 195–205.

(23) Muro, M. L.; Rachford, A. A.; Wang, X.; Castellano, F. N. PlatinumII Acetylide Photophysics. In *Photophysics of Organometallics*; Lees, A. J., Ed.; Springer: Berlin, Heidelberg, 2010; pp 1–35.

(24) Hua, F.; Kinayyigit, S.; Cable, J. R.; Castellano, F. N. Platinum(II) Diimine Diacetylides: Metallacyclization Enhances Photophysical Properties. *Inorg. Chem.* **2006**, *45* (11), 4304–4306.

(25) Castellano, F. N.; Pomestchenko, I. E.; Shikhova, E.; Hua, F.; Muro, M. L.; Rajapakse, N. Photophysics in Bipyridyl and Terpyridyl Platinum(II) Acetylides. *Coord. Chem. Rev.* **2006**, *250* (13-14), 1819–1828.

(26) Wang, X.; Goeb, S.; Ji, Z.; Castellano, F. N. Excited State Absorption Properties of Pt(II) Terpyridyl Complexes Bearing π-Conjugated Arylacetylides. *J. Phys. Chem. B* **2010**, *114* (45), 14440–14449.

(27) Cho, S.; Mara, M. W.; Wang, X.; Lockard, J. V.; Rachford, A. A.; Castellano, F. N.; Chen, L. X. Coherence in Metal−Metal-to-Ligand-Charge-Transfer Excited States of a Dimetallic Complex Investigated by Ultrafast Transient Absorption Anisotropy. *J. Phys. Chem. A* **2011**, *115* (16), 3990–3996.

(28) Castellano, F. N. Altering Molecular Photophysics by Merging Organic and Inorganic Chromophores. *Acc. Chem. Res.* **2015**, *48* (3), 828–839.

(29) Brown-Xu, S. E.; Kelley, M. S. J.; Fransted, K. A.; Chakraborty, A.; Schatz, G. C.; Castellano, F. N.; Chen, L. X. Tunable Excited-State Properties and Dynamics as a Function of Pt–Pt Distance in Pyrazolate-Bridged Pt(II) Dimers. *J. Phys. Chem. A* **2016**, *120* (4), 543–550.

(30) Hoijtink, G. J. The Influence of Paramagnetic Molecules on Singlet-Triplet Transitions. *Mol. Phys.* **1960**, *3* (1), 67–70.

(31) Chiu, Y.-N. On Singlet-Triplet Transitions Induced by Exchange with Paramagnetic Molecules and the Intermolecular Coupling of Spin Angular Momenta. *J. Chem. Phys.* **1972**, *56* (10), 4882–4898.

(32) J. Gijzeman, O. L. J.; Kaufman, F.; Porter, G. Oxygen Quenching of Aromatic Triplet States in Solution. Part 1. *J. Chem. Soc., Faraday Trans. 2 Mol. Chem. Phys.* **1973**, *69* (0), 708–720.

(33) Fudickar, W.; Linker, T. Reversible Photooxygenation of Alkynylanthracenes: Chemical Generation of Singlet Oxygen under Very Mild Conditions. *Chem. – Eur. J.* **2011**, *17* (49), 13661–13664.

(34) Yanai, N.; Kimizuka, N. Recent Emergence of Photon Upconversion Based on Triplet Energy Migration in Molecular Assemblies. *Chem. Commun.* **2016**, *52* (31), 5354–5370.

(35) Kimizuka, N.; Yanai, N.; Morikawa, M. Photon Upconversion and Molecular Solar Energy Storage by Maximizing the Potential of Molecular Self-Assembly. *Langmuir* **2016**, *32* (47), 12304–12322.

(36) Tilley, A. J.; Robotham, B. E.; Steer, R. P.; Ghiggino, K. P. Sensitized Non-Coherent Photon Upconversion by Intramolecular Triplet–Triplet Annihilation in a Diphenylanthracene Pendant Polymer. *Chem. Phys. Lett.* **2015**, *618*, 198–202.

(37) Gray, V.; Dzebo, D.; Lundin, A.; Alborzpour, J.; Abrahamsson, M.; Albinsson, B.; Moth-Poulsen, K. Photophysical Characterization of the 9,10-Disubstituted Anthracene Chromophore and Its Applications in Triplet–Triplet Annihilation Photon Upconversion. *J. Mater. Chem. C* **2015**, *3* (42), 11111–11121.

(38) Pun, A. B.; Sanders, S. N.; Sfeir, M. Y.; Campos, L. M.; Congreve, D. N. Annihilator Dimers Enhance Triplet Fusion Upconversion. *Chem. Sci.* **2019**, *10* (14), 3969–3975.

(39) Deng, F.; Sommer, J. R.; Myahkostupov, M.; Schanze, K. S.; Castellano, F. N. Near-IR Phosphorescent Metalloporphyrin as a Photochemical Upconversion Sensitizer. *Chem. Commun.* **2013**, *49* (67), 7406.

(40) Sugunan, S. K.; Tripathy, U.; Brunet, S. M. K.; Paige, M. F.; Steer, R. P. Mechanisms of Low-Power Noncoherent Photon Upconversion in Metalloporphyrin−Organic Blue Emitter Systems in Solution. *J. Phys. Chem. A* **2009**, *113* (30), 8548–8556.

(41) Giri, N. K.; Ponce, C. P.; Steer, R. P.; Paige, M. F. Homomolecular Non-Coherent Photon Upconversion by Triplet–Triplet Annihilation Using a Zinc Porphyrin on Wide Bandgap Semiconductors. *Chem. Phys. Lett.* **2014**, *598*, 17–22.

(42) Steer, R. P. Prospects for Efficient Solar Energy Upconversion Using Metalloporphyrins as Dual Absorber-Upconverters. *Dalton Trans.* **2018**, *47* (26), 8517–8525.

(43) Hagstrom, A. L.; Deng, F.; Kim, J.-H. Enhanced Triplet–Triplet Annihilation Upconversion in Dual-Sensitizer Systems: Translating Broadband Light Absorption to Practical Solid-State Materials. *ACS Photonics* **2017**, *4* (1), 127–137.

(44) Ye, C.; Wang, J.; Wang, X.; Ding, P.; Liang, Z.; Tao, X. A New Medium for Triplet–Triplet Annihilated Upconversion and Photocatalytic Application. *Phys. Chem. Chem. Phys.* **2016**, *18* (5), 3430–3437.

(45) Liu, N.; Chen, H.; Su, J.; Weng, Y.; Vittal, J. J.; Huang, S.-L.; Jiang, J. Porphyrin–Sensitizers and Anthracene–Annihilators Built in Isostructural Frameworks for Investigating Triplet–Triplet Annihilation Upconversion. *Inorg. Chem.* **2024**, *63* (10), 4691–4696.

(46) Singh-Rachford, T. N.; Castellano, F. N. Supra-Nanosecond Dynamics of a Red-to-Blue Photon Upconversion System. *Inorg. Chem.* **2009**, *48* (6), 2541–2548.

(47) Olivier, J.-H.; Bai, Y.; Uh, H.; Yoo, H.; Therien, M. J.; Castellano, F. N. Near-Infrared-to-Visible Photon Upconversion Enabled by Conjugated Porphyrinic Sensitizers under Low-Power Noncoherent Illumination. *J. Phys. Chem. A* **2015**, *119* (22), 5642–5649.

(48) Tripathy, U.; Steer, R. P. The Photophysics of Metalloporphyrins Excited in Their Soret and Higher Energy UV Absorption Bands. *J. Porphyrins Phthalocyanines* **2007**, *11* (04), 228–243.

(49) Min Park, J.; Lee, J. H.; Jang, W.-D. Applications of Porphyrins in Emerging Energy Conversion Technologies. *Coord. Chem. Rev.* **2020**, *407*, 213157.

(50) Parker, C. A.; Hatchard, C. G. Delayed Fluorescence from Solutions of Anthracene and Phenanthrene. *Proc. R. Soc. A* **1962**, *269* (1339), 574-584.

(51) Kozlov, D. V.; Castellano, F. N. Anti-Stokes Delayed Fluorescence from Metal–Organic Bichromophores. *Chem. Commun.* **2004**, *24*, 2860–2861.

(52) Islangulov, R. R.; Kozlov, D. V.; Castellano, F. N. Low Power Upconversion Using MLCT Sensitizers. *Chem. Commun.* **2005**, *30*, 3776–3778.

(53) Keivanidis, P. E.; Baluschev, S.; Miteva, T.; Nelles, G.; Scherf, U.; Yasuda, A.; Wegner, G. Up-Conversion Photoluminescence in Polyfluorene Doped with Metal(II)–Octaethyl Porphyrins. *Adv. Mater.* **2003**, *15* (24), 2095–2098.

(54) Baluschev, S.; Keivanidis, P. E.; Wegner, G.; Jacob, J.; Grimsdale, A. C.; Müllen, K.; Miteva, T.; Yasuda, A.; Nelles, G. Upconversion Photoluminescence in Poly(Ladder-Type-Pentaphenylene) Doped with Metal (II)-Octaethyl Porphyrins. *Appl. Phys. Lett.* **2005**, *86* (6), 061904.

(55) Baluschev, S.; Jacob, J.; Avlasevich, Y. S.; Keivanidis, P. E.; Miteva, T.; Yasuda, A.; Nelles, G.; Grimsdale, A. C.; Müllen, K.; Wegner, G. Enhanced Operational Stability of the Up-

Conversion Fluorescence in Films of Palladium–Porphyrin End-Capped Poly(Pentaphenylene). *ChemPhysChem* **2005**, *6* (7), 1250–1253.

(56) Naimovičius, L.; Bharmoria, P.; Moth-Poulsen, K. Triplet–Triplet Annihilation Mediated Photon Upconversion Solar Energy Systems. *Mater. Chem. Front.* **2023**, *7* (12), 2297–2315.

(57) Huang, L.; Le, T.; Huang, K.; Han, G. Enzymatic Enhancing of Triplet–Triplet Annihilation Upconversion by Breaking Oxygen Quenching for Background-Free Biological Sensing. *Nat. Commun.* **2021**, *12* (1), 1898.

(58) Huang, L.; Zeng, L.; Chen, Y.; Yu, N.; Wang, L.; Huang, K.; Zhao, Y.; Han, G. Long Wavelength Single Photon like Driven Photolysis via Triplet Triplet Annihilation. *Nat. Commun.* **2021**, *12* (1), 122.

(59) Bharmoria, P.; Bildirir, H.; Moth-Poulsen, K. Triplet–Triplet Annihilation Based near Infrared to Visible Molecular Photon Upconversion. *Chem. Soc. Rev.* **2020**, *49* (18), 6529–6554.

(60) Zhou, J.; Liu, Q.; Feng, W.; Sun, Y.; Li, F. Upconversion Luminescent Materials: Advances and Applications. *Chem. Rev.* **2015**, *115* (1), 395–465.

(61) Huang, L.; Wu, W.; Li, Y.; Huang, K.; Zeng, L.; Lin, W.; Han, G. Highly Effective Near-Infrared Activating Triplet–Triplet Annihilation Upconversion for Photoredox Catalysis. *J. Am. Chem. Soc.* **2020**, *142* (43), 18460–18470.

(62) Castellanos-Soriano, J.; Zähringer, T. J. B.; Herrera-Luna, J. C.; Jiménez, M. C.; Kerzig, C.; Pérez-Ruiz, R. A New Green-to-Blue Upconversion System with Efficient Photoredox Catalytic Properties. *Phys. Chem. Chem. Phys.* **2023**, *25* (17), 12041–12049.

(63) Glaser, F.; Kerzig, C.; Wenger, O. S. Multi-Photon Excitation in Photoredox Catalysis: Concepts, Applications, Methods. *Angew. Chem. Int. Ed.* **2020**, *59* (26), 10266–10284.

(64) Awwad, N.; Bui, A. T.; Danilov, E. O.; Castellano, F. N. Visible-Light-Initiated Free-Radical Polymerization by Homomolecular Triplet-Triplet Annihilation. *Chem* **2020**, *6* (11), 3071–3085.

(65) Limberg, D. K.; Kang, J.-H.; Hayward, R. C. Triplet–Triplet Annihilation Photopolymerization for High-Resolution 3D Printing. *J. Am. Chem. Soc.* **2022**, *144* (12), 5226–5232.

(66) Sanders, S. N.; Schloemer, T. H.; Gangishetty, M. K.; Anderson, D.; Seitz, M.; Gallegos, A. O.; Stokes, R. C.; Congreve, D. N. Triplet Fusion Upconversion Nanocapsules for Volumetric 3D Printing. *Nature* **2022**, *604* (7906), 474–478.

(67) Kasha, M. Characterization of Electronic Transitions in Complex Molecules. *Discuss. Faraday Soc.* **1950**, *9* (0), 14–19.

(68) Maciejewski, A.; Steer, R. P. The Photophysics, Physical Photochemistry, and Related Spectroscopy of Thiocarbonyls. *Chem. Rev.* **1993**, *93* (1), 67–98.

(69) Itoh, T. Fluorescence and Phosphorescence from Higher Excited States of Organic Molecules. *Chem. Rev.* **2012**, *112* (8), 4541–4568.

(70) Stelmakh, G. F; Tsvirko, M. P. Delayed Fluorescence from the Upper Excited Electronic States of Metalloporphyrins. *Opt. Spectrosc.* **1980**, *49* (3), 278–281.

(71) Stelmakh, G. F.; Tsvirko, M. P. Metalloporphyrin Dimeric S2 Emission Resulting from Triplet-Triplet Annihilation. *ACS Symp. Ser.* **1986**, *321*, 118-127.

(72) Steer, R. P. Electronic Energy-Pooling Processes in Polyatomic Molecules. *Res. Chem. Intermed.* **1989**, *12* (1), 81–101.

(73) Olesund, A.; Gray, V.; Mårtensson, J.; Albinsson, B. Diphenylanthracene Dimers for Triplet–Triplet Annihilation Photon Upconversion: Mechanistic Insights for Intramolecular Pathways and the Importance of Molecular Geometry. *J. Am. Chem. Soc.* **2021**, *143* (15), 5745–5754.

(74) Kim, D.; Kirmaier, C.; Holten, D. Nickel Porphyrin Photophysics and Photochemistry. A Picosecond Investigation of Ligand Binding and Release in the Excited State. *Chem. Phys.* **1983**, *75* (3), 305–322.

(75) Drain, C. M.; Kirmaier, C.; Medforth, C. J.; Nurco, D. J.; Smith, K. M.; Holten, D. Dynamic Photophysical Properties of Conformationally Distorted Nickel Porphyrins. 1. Nickel(II) Dodecaphenylporphyrin. *J. Phys. Chem.* **1996**, *100* (29), 11984–11993.

(76) Antipas, A.; Gouterman, M. Porphyrins. 44. Electronic States of Cobalt, Nickel, Rhodium, and Palladium Complexes. *J. Am. Chem. Soc.* **1983**, *105* (15), 4896–4901.

(77) Koga, M.; Sotome, H.; Ide, N.; Ito, S.; Nagasawa, Y.; Miyasaka, H. Direct Determination of Molar Absorption Coefficients of Several Molecules in the Lowest Excited Singlet States. *Photochem. Photobiol. Sci.* **2021**, *20* (10), 1287–1297.

(78) Kalyanasundaram, K. *Photochemistry of Polypyridine and Porphyrin Complexes*; Academic Press: London, UK, 1991.

(79) Gurzadyan, G. G.; Tran-Thi, T.-H.; Gustavsson, T. Direct Measurement of S2 -- S0 Fluorescence Lifetimes and Anisotropy of Tetraphenylporphyrins. In *New Trends in Atomic and Molecular Spectroscopy*; Gurzadyan, G. G., Karmenyan, A. V., Eds.; SPIE: Russia, 1999; p 96.

(80) Hirakawa, K.; Saito, K.; Segawa, H. Anomalously Selective Quenching of S2 Fluorescence from Upper Excited State of Zinc 5-(1′-Pyrenyl)-10,15,20-Triphenylporphyrin Derivatives through Intramolecular Charge Transfer State. *J. Phys. Chem. A* **2009**, *113* (31), 8852–8856.

(81) Morandeira, A.; Engeli, L.; Vauthey, E. Ultrafast Charge Recombination of Photogenerated Ion Pairs to an Electronic Excited State. *J. Phys. Chem. A* **2002**, *106* (19), 4833–4837.

(82) Borek, C.; Hanson, K.; Djurovich, P. I.; Thompson, M. E.; Aznavour, K.; Bau, R.; Sun, Y.; Forrest, S. R.; Brooks, J.; Michalski, L.; et al. Highly Efficient, Near-Infrared Electrophosphorescence from a Pt–Metalloporphyrin Complex. *Angew. Chem., Int. Ed.* **2007**, *46* (7), 1109–1112.

(83) Liu, L.; Han, B.; Cao, Y.; Wen, J. The Influence of Non-Radiative Relaxation on the Room-Temperature Phosphorescence of Metalloporphyrin. *J. Porphyrins Phthalocyanines* **2022**, *26* (12), 884–890.

(84) Hilpern, J. W.; Porter, G.; Stief, L. J. Decay of the Triplet State I. First-Order Processes in Solution. *Proc. R. Soc. A.* **1964**, *277* (1371), 437–447.

(85) Bachilo, S. M.; Weisman, R. B. Determination of Triplet Quantum Yields from Triplet−Triplet Annihilation Fluorescence. *J. Phys. Chem. A* **2000**, *104* (33), 7711–7714.

(86) Deng, F.; Blumhoff, J.; Castellano, F. N. Annihilation Limit of a Visible-to-UV Photon Upconversion Composition Ascertained from Transient Absorption Kinetics. *J. Phys. Chem. A* **2013**, *117* (21), 4412–4419.

(87) Montalti, M.; Credi, A.; Prodi, L.; Gandolfi, M. T. *Handbook of Photochemistry*, 3rd ed.; CRC Press: Boca Raton, 2006.

(88) Ballard, S. G.; Mauzerall, D. C. Photochemical Ionogenesis in Solutions of Zinc Octaethyl Porphyrin. *J. Chem. Phys.* **1980**, *72* (2), 933–947.

Supporting Information

Femtosecond Transient Absorption Spectroscopy

Femtosecond transient absorption spectroscopy was performed at the Imaging and Kinetic Spectroscopy (IMAKS) Laboratory at NCSU. For femtosecond transient absorption measurements, samples had ground state absorptions ranging from 0.3 to 0.5 optical density (OD) at their respective Soret Band maxima. All solutions used in the photophysical measurements were prepared using spectroscopic grade toluene. The apparatus included a 1 kHz Ti:Sapphire Coherent Libra regenerative amplifier to generate an initial 800 nm beam, split into pump and probe beams. The pump beam, from an OperA Solo parametric amplifier (Coherent), was focused within an Ultrafast Systems Helios transient absorption spectrometer. The probe beam was generated by focusing the remaining 800 nm output through a sapphire crystal to create a white light continuum. In the spectrometer, the overlap of pump and probe beams was achieved within a 2 mm pathlength cuvette.

Samples were excited at wavelengths corresponding to the respective Q band maxima. For transient absorption difference spectra, samples exhibited a linear ΔA-pulse energy relationship (Figure S2.5). Throughout each experiment, samples were stirred continuously, and static UV-Vis spectroscopy was conducted before and after each experiment to confirm sample integrity and absence of decomposition. Due to the high ISC efficiency in these heavy metal-centered porphyrins, it we assumed that nearly all the excited state singlets convert to excited state triplets. This characteristic allowed us to conveniently apply the Beer-Lambert Law. By measuring the ΔA (OD) of the ground state bleach feature, we calculated the concentration of the excited state triplets. Subsequently, we correlated this with the ΔA of the triplet absorption feature to determine the triplet extinction coefficient (ε_t).

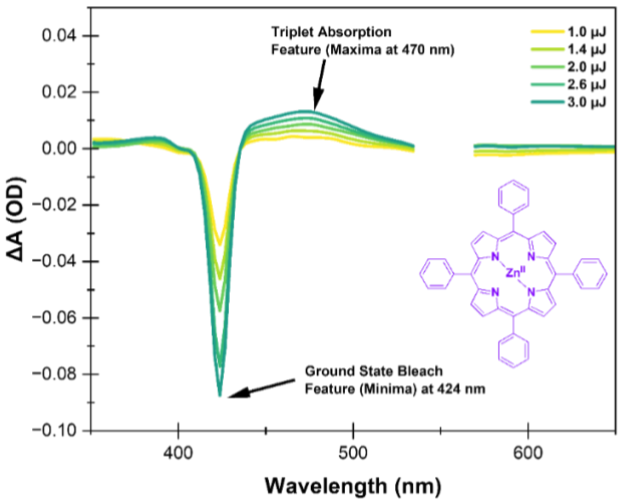

Figure S0.1 Femtosecond transient absorption difference spectra for ZnTPP in toluene after photoexcitation at 550 nm at various pulse energies (indicated in the legend).

Table S0.1 Calculation for the Determination of the Triplet Extinction Coefficient ($\varepsilon_{t\ (470\ nm)}$) of ZnTPP in Toluene Using fs-TA Data (Figure S2.1).[a]

Pulse Energy (µJ)	ΔA (OD) at Bleach (424 nm – B Band)	$C_g = \frac{\Delta A\ (424\ nm)}{\varepsilon_g * l}$ (10^{-7} M)	ΔA (OD) at Triplet Signature (473 nm)	$\varepsilon_{t\ (470\ nm)} = \frac{\Delta A\ (470\ nm)}{c_g * l}$ (10^4 $M^{-1}cm^{-1}$)
1.0	-0.0341	3.0	0.0040	6.6
1.4	-0.0461	4.1	0.0063	7.6
2.0	-0.0574	5.1	0.0087	8.5
2.6	-0.0772	6.9	0.0109	7.9
3.0	-0.0875	7.8	0.0132	8.4

[a]Ground state extinction coefficient (ε_g) for the B band in ZnTPP = 5.6 x 10^5 $M^{-1}cm^{-1}$, path length (l) = 0.2 cm. Average triplet extinction coefficient for ZnTPP in toluene = 78000 M^{-1} cm^{-1}.

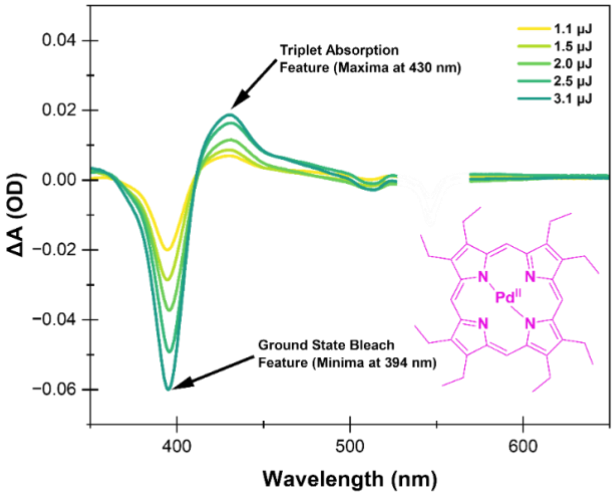

Figure S0.2 Femtosecond transient absorption difference spectra for PdOEP in toluene after photoexcitation at 547 nm at various pulse energies (indicated in the legend).

Table S0.2 Calculation for the Determination of the Triplet Extinction Coefficient ($\varepsilon_{t\ (430\ nm)}$) of PdOEP in Toluene Using fs-TA Data (Figure S2.2).[b]

Pulse Energy (µJ)	ΔA (OD) at Bleach (394 nm – B Band)	$C_g = \frac{\Delta A\ (394\ nm)}{\varepsilon_g * l}$ (10^{-7} M)	ΔA (OD) at Triplet Signature (430 nm)	$\varepsilon_{t\ (430\ nm)} = \frac{\Delta A\ (430\ nm)}{c_g * l}$ (10^4 $M^{-1}cm^{-1}$)
1.1	-0.0200	4.8	0.0070	7.3
1.5	-0.0286	6.8	0.0086	6.3
2.0	-0.0367	8.7	0.0115	6.6
2.5	-0.0483	11.5	0.0163	7.1
3.1	-0.0597	14.2	0.0187	6.6

[b]Ground state extinction coefficient (ε_g) for the B band in PdOEP = 2.1 x 10^5 $M^{-1}cm^{-1}$, path length (l) = 0.2 cm. Average triplet extinction coefficient for PdOEP in toluene at 430 nm = 67000 M^{-1} cm^{-1}.

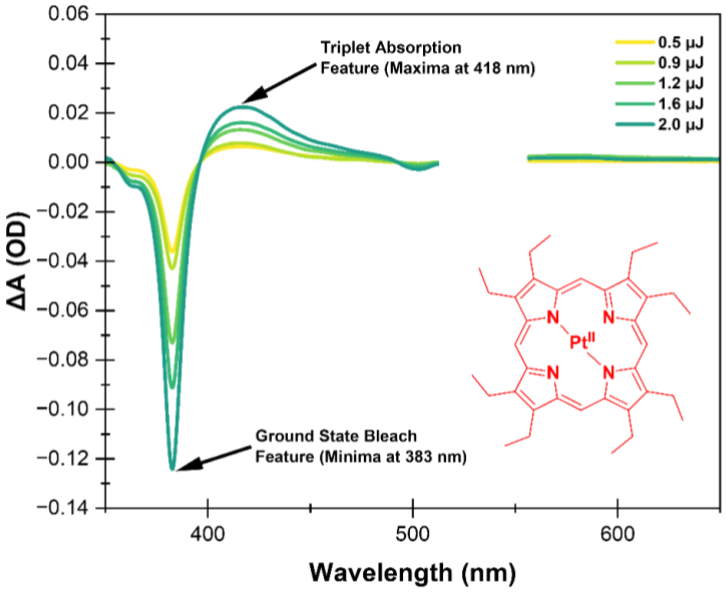

Figure S0.3 Femtosecond transient absorption difference spectra for PtOEP in toluene after photoexcitation at 535 nm at various pulse energies (indicated in the legend).

Table S0.3 Calculation for the Determination of the Triplet Extinction Coefficient ($\varepsilon_{t\ (418\ nm)}$) of PtOEP in Toluene Using fs-TA Data (Figure S2.3).[c]

Pulse Energy (µJ)	ΔA (OD) at Bleach (383 nm – B Band)	$C_g = \frac{\Delta A\ (383\ nm)}{\varepsilon_g * l}$ (10^{-7} M)	ΔA (OD) at Triplet Signature (418 nm)	$\varepsilon_{t\ (418\ nm)} = \frac{\Delta A\ (418\ nm)}{c_g * l}$ (10^4 $M^{-1}cm^{-1}$)
0.9	-0.0423	7.6	0.0078	5.1
1.2	-0.0718	12.8	0.0131	5.1
1.6	-0.0897	16.0	0.0160	5.0
2.0	-0.1222	21.8	0.0223	5.1

[c]Ground state extinction coefficient (ε_g) for the B band in PtOEP = 2.8 x 10^5 $M^{-1}cm^{-1}$, path length (l) = 0.2 cm. Average triplet extinction coefficient for PtOEP in toluene at 418 nm = 51000 M^{-1} cm^{-1}.

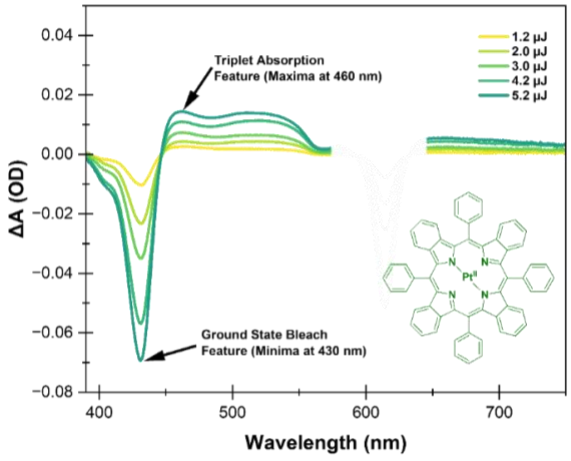

Figure S0.4 Femtosecond transient absorption difference spectra for PtTPBP in toluene after photoexcitation at 615 nm at various pulse energies (indicated in the legend).

Table S0.4 Calculation for the Determination of the Triplet Extinction Coefficient ($\varepsilon_{t\ (460\ nm)}$) of PtTPBP in Toluene Using fs-TA Data (Figure S2.4).[d]

Pulse Energy (µJ)	ΔA (OD) at Bleach (430 nm – B Band)	$C_g = \frac{\Delta A\ (430\ nm)}{\varepsilon_g * l}$ (10^{-7} M)	ΔA (OD) at Triplet Signature (460 nm)	$\varepsilon_T = \frac{\Delta A\ (460\ nm)}{c_g * l}$ (10^4 $M^{-1}cm^{-1}$)
1.2	-0.0102	1.0	0.0026	12
2.0	-0.0229	2.3	0.0043	9.1
3.0	-0.0347	3.5	0.0073	10
4.2	-0.0566	5.8	0.0110	9.5
5.2	-0.0690	7.0	0.0143	10

[d]Ground state extinction coefficient (ε_g) for the B band in PtTPBP = 4.9 x 10^5 $M^{-1}cm^{-1}$, path length (l) = 0.2 cm. Average triplet extinction coefficient for PtTPBP in toluene at 460 nm = 100000 M^{-1} cm^{-1}.

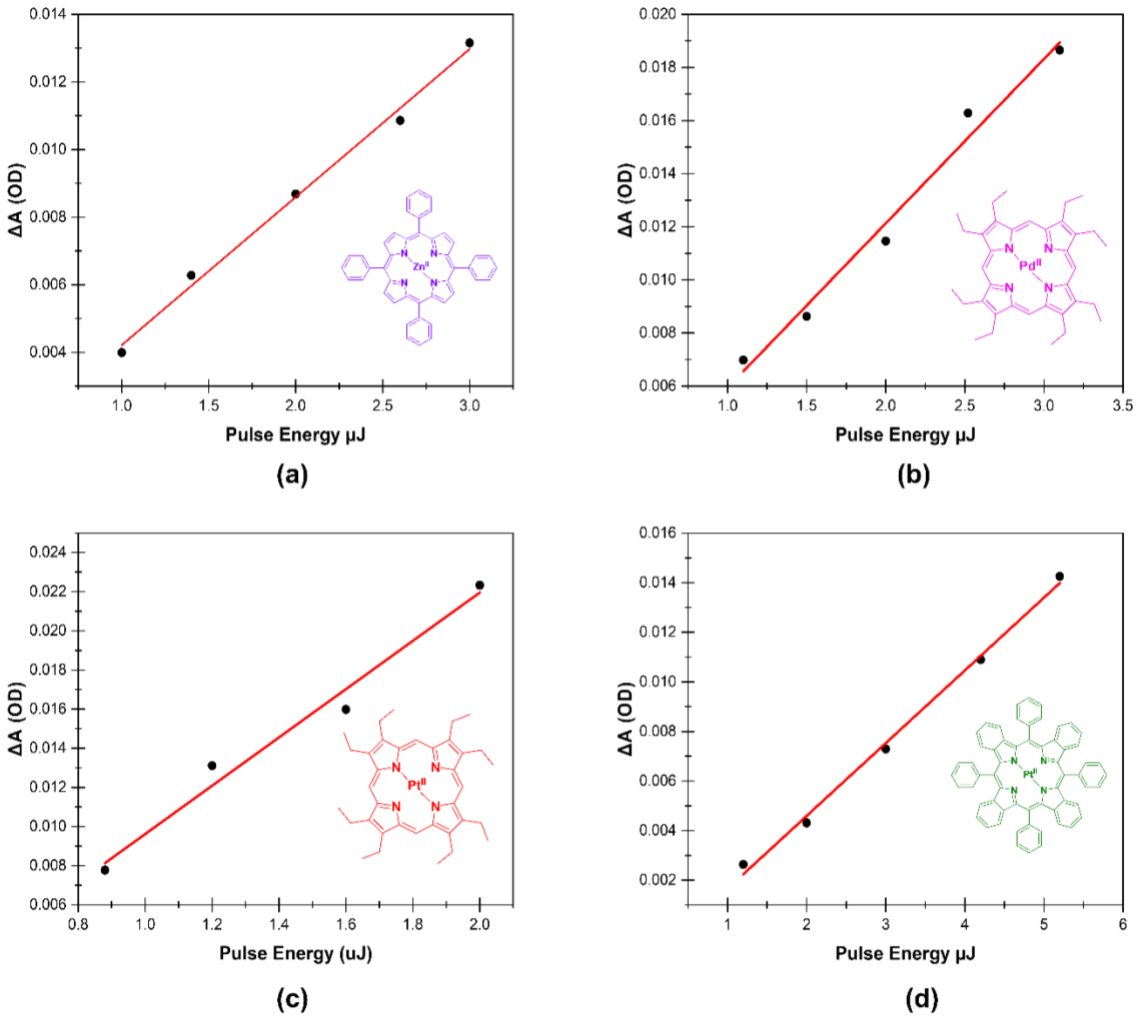

Figure S0.5 Linear plots for the femtosecond transient absorption difference spectra to ensure that ΔA remained linear within the power regime under study (a) ZnTPP (photoexcitation at 550 nm), (b) PdOEP (photoexcitation at 547 nm), (c) PtOEP (photoexcitation at 53535 nm), (d) PtTPBP (photoexcitation at 615 nm).

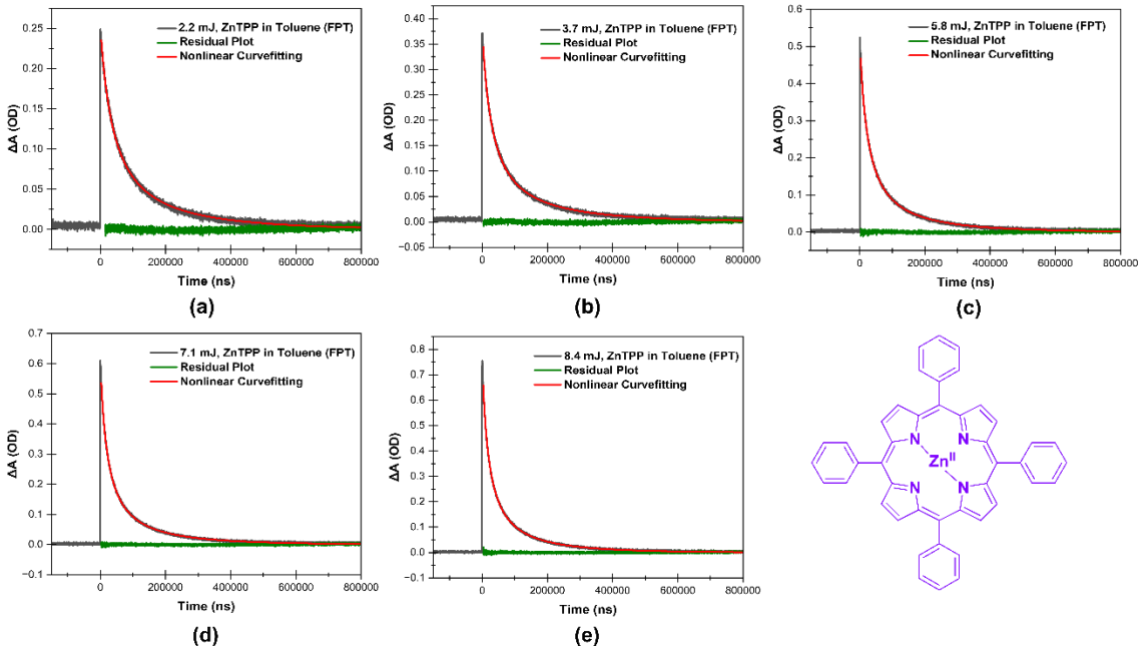

Figure S0.6 Nanosecond transient absorption kinetic decays (black) of triplet ZnTPP at 470 nm produced using 514 nm excitation at variable pulse energies (indicated in the legend) in 0.05 mM of ZnTPP in freeze-pump-thaw degassed toluene. The red line represents the kinetic fit to eq 2.3 (refer to the main text) and the green indicates the residuals of the fit.

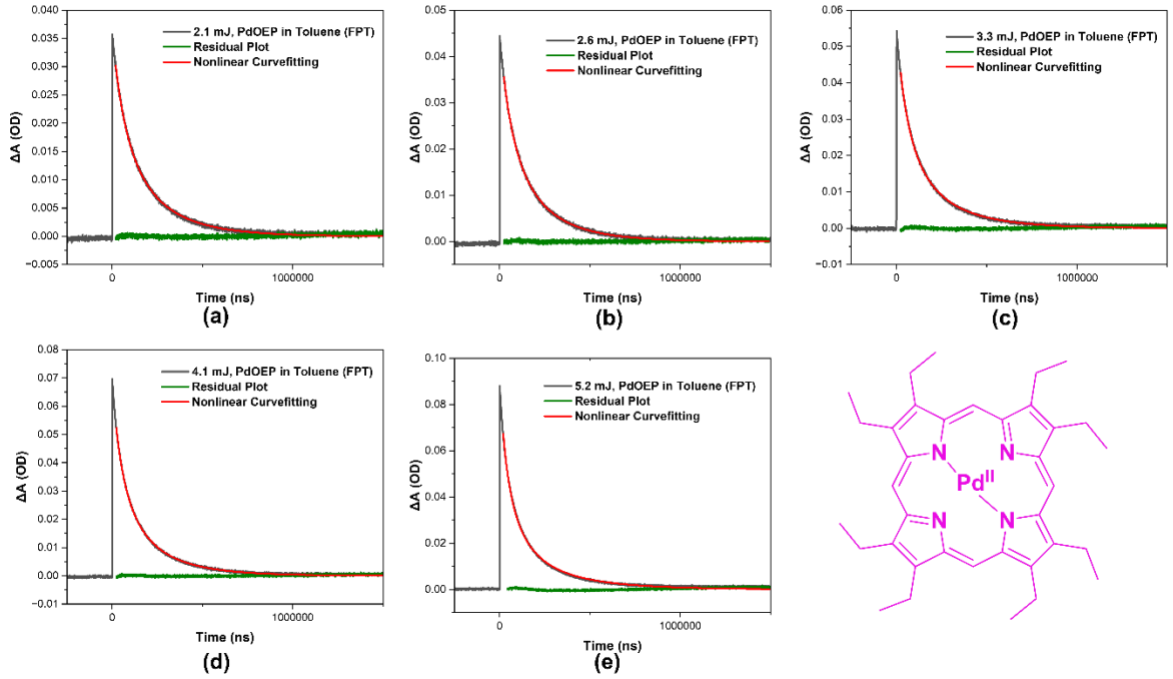

Figure S0.7 Nanosecond transient absorption kinetic decays (black) of triplet PdOEP at 430 nm produced using 514 nm excitation at variable pulse energies (indicated in the legend) in 0.05 mM of PdOEP in freeze-pump-thaw degassed toluene. The red line represents the kinetic fit to eq 2.3 (refer to the main text) and the green indicates the residuals of the fit.

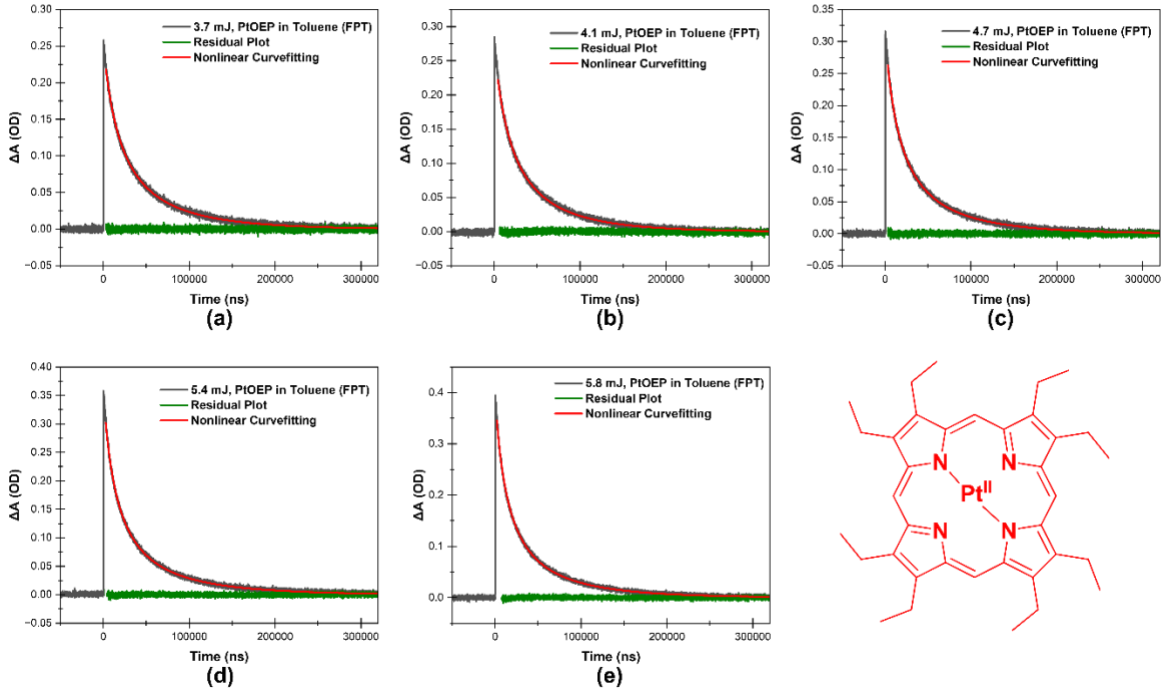

Figure S0.8 Nanosecond transient absorption kinetic decays (black) of triplet PtOEP at 418 nm produced using 514 nm excitation at variable pulse energies (indicated in the legend) in 0.05 mM of PtOEP in freeze-pump-thaw degassed toluene. The red line represents the kinetic fit to eq 2.3 (refer to the main text) and the green indicates the residuals of the fit.

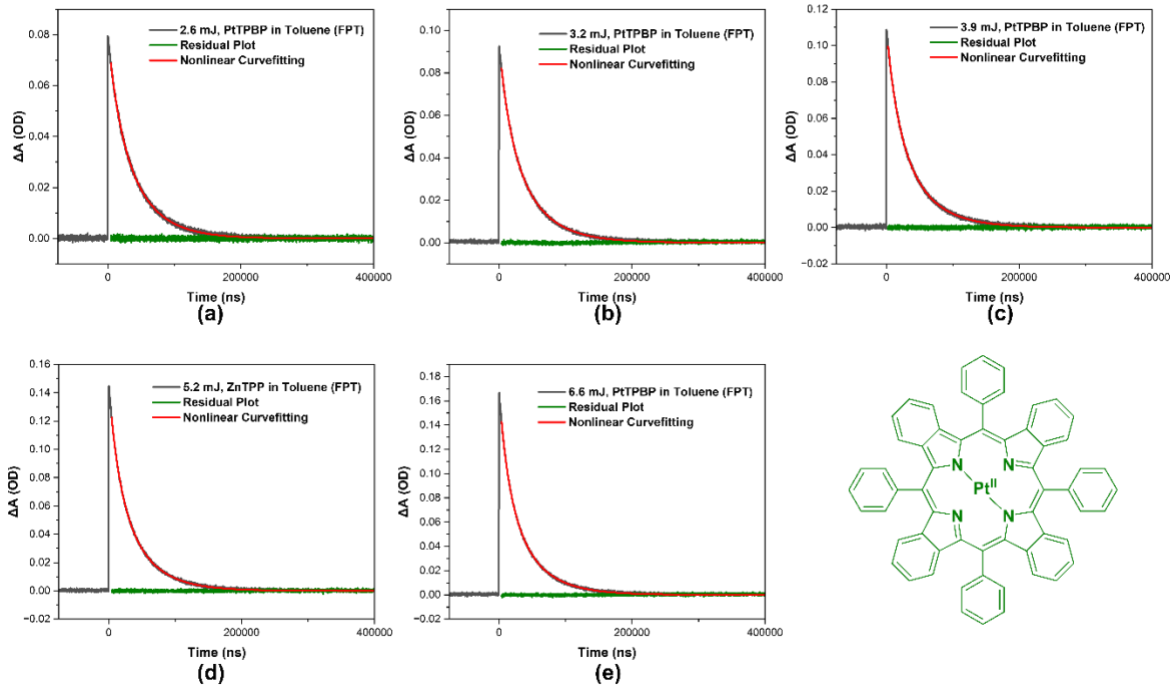

Figure S0.9 Nanosecond transient absorption kinetic decays (black) of triplet PtTPBP at 460 nm produced using 560 nm excitation at variable pulse energies (indicated in the legend) in 0.05 mM of ZnTPP in freeze-pump-thaw degassed toluene. The red line represents the kinetic fit to eq 2.3 (refer to the main text) and the green indicates the residuals of the fit.

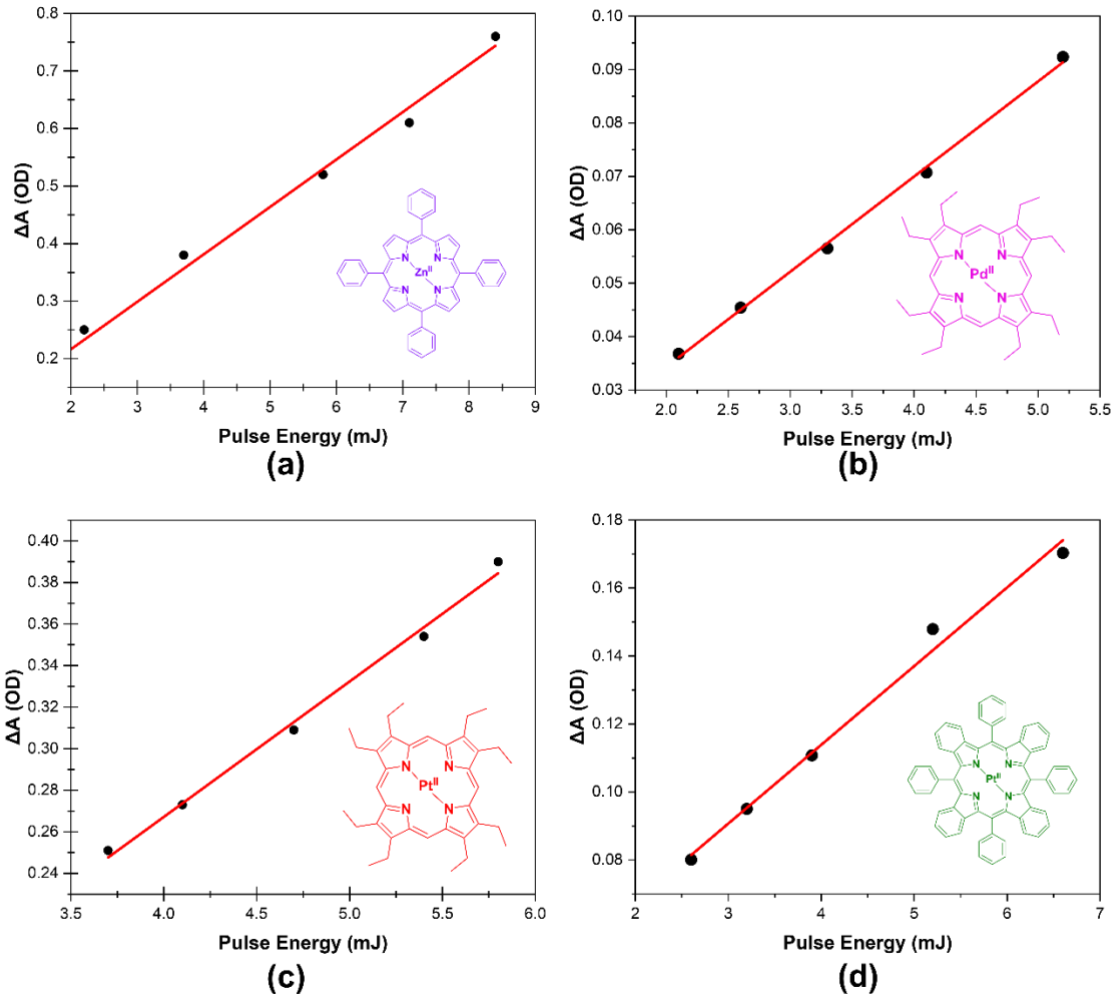

Figure S0.10 Linear plots for the nanosecond transient absorption difference spectra to ensure that ΔA remained linear within the power regime under study (a) ZnTPP (photoexcitation at 514 nm), (b) PdOEP (photoexcitation at 514 nm), (c) PtOEP (photoexcitation at 514 nm), (d) PtTPBP (photoexcitation at 560 nm).

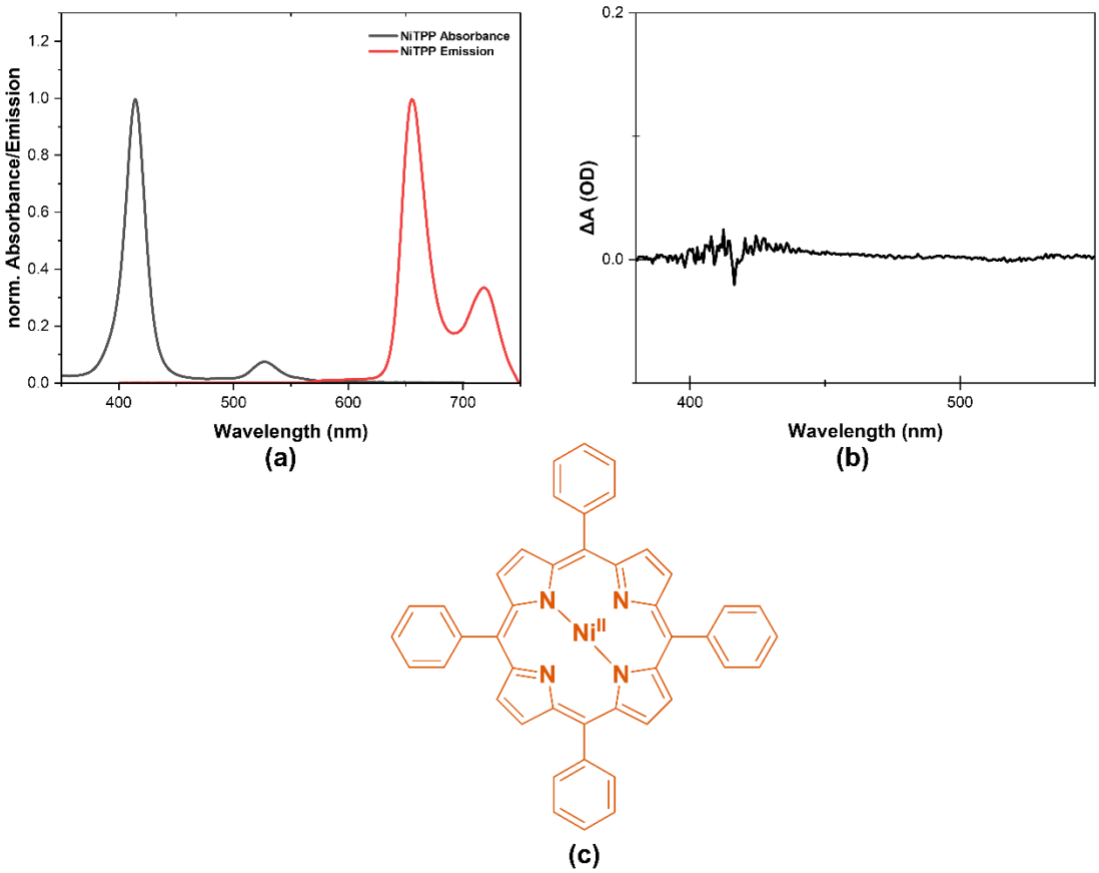

Figure S0.11 (a) Room temperature normalized absorption and emission spectra for nickel(II) tetraphenylporphyrin (NiTPP), (b) Prompt nanosecond transient absorption difference spectrum of NiTPP (0.05 mM in freeze-pump-thaw degassed toluene) after photoexcitation at 514 nm (3 mJ, 5-7 ns fwhm), (c) Chemical structure of NiTPP.